

Andreas Mutzke, Ralf Schneider, Wolfgang Eckstein, Renate Dohmen

**SDTrimSP Version 5.00**

**IPP 12/8**  
April, 2011

# SDTrimSP Version 5.00

A. Mutzke, R. Schneider, W. Eckstein, R. Dohmen

## Abstract

SDTrimSP version 5.00 is designed for atomic collisions in amorphous targets to calculate ranges, reflection coefficients and sputtering yields as well as more detailed information as depth distributions of implanted and energy distributions of backscattered and sputtered atoms. The program is based on the binary collision approximation and uses the same physics as its predecessors TRIM.SP and TRIDYN, but the structure of the new program has been completely changed. It runs on all sequential and parallel platforms with a F90 compiler. Table lookup is applied for all available atomic data needed for input, and different integration schemes for several interaction potentials are provided. Selected examples of typical results are given to show the manifold of possible applications.

This report replaces the previous version (IPP 12/3).

# Contents

<b>1. Introduction</b>	<b>4</b>
<b>2. Physical basis</b>	<b>5</b>
<b>3. Structure of the code</b>	<b>6</b>
<b>4. Implementation</b>	<b>9</b>
<b>5. Performance</b>	<b>10</b>
5.1. Influence of NR and NH on the accuracy of the results . . . . .	11
5.2. Parallel efficiency . . . . .	13
<b>6. Special applications</b>	<b>16</b>
6.1. Static mode . . . . .	16
6.2. Dynamic mode . . . . .	19
<b>7. Extension in Version 5.00</b>	<b>23</b>
7.1. Sputtering with noble gas ions . . . . .	23
7.2. Chemical erosion of carbon . . . . .	28
<b>8. Sensitivity studies for D on Be and D on W</b>	<b>33</b>
8.1. Number of incident particles . . . . .	33
8.2. Surface binding energy . . . . .	35
8.3. Integration methods . . . . .	39
8.4. Sreened coulomb potentials . . . . .	42
<b>9. New input variables in 'tri.inp'</b>	<b>45</b>
<b>A. Global parameters</b>	<b>48</b>
<b>B. Input variables in 'tri.inp'</b>	<b>48</b>
B.1. Necessary input variables . . . . .	48
B.2. Optional input variables . . . . .	50
B.3. Output format of energy distribution in the target . . . . .	58
B.4. Output format of the depth of origin and penetration depth . . . . .	58
B.5. Output format of energy- and angle-distribution of scattered and sput- tered atoms . . . . .	59
B.5.1. Output-matrix-file . . . . .	59
B.5.2. Post-processing of output-matrix-file with readmatrix4.F90 . . . . .	59
<b>C. Inputfile 'layer.inp'</b>	<b>61</b>
<b>D. Inputfiles 'energy.inp' and angle.inp</b>	<b>62</b>

<b>E. Inputfiles 'ene_ang.inp'</b>	<b>63</b>
<b>F. Example of new Inputfile 'tri.inp'</b>	<b>64</b>

# 1. Introduction

In the last 40 years many computer simulation programs have been developed to describe the interactions of ions bombarding solid, liquid and gaseous targets. Many of these programs were based on the binary-collision approximation dealing with crystalline and amorphous targets. Examples of programs dealing with amorphous targets are the static Monte-Carlo program TRIM and the corresponding dynamic version TRIDYN which were successful in describing collision effects in solids for many examples [1]. Many versions of these two programs evolved to handle specific physical problems. This triggered the idea to combine both programs in a new version SDTrimSP (where S stands for static and D for dynamic) with all possible output facilities used in the past like sputtering, backscattering and transmission. This offered the opportunity to introduce at the same time a modular structure, to have a more flexible output and to provide a higher portability. The program is suited equally well for all sequential architectures and for all parallel architectures, for which a Fortran 90 (F90) compiler and the MPI (Message Passing Interface) communication library are available. The new program also includes features which were used in the past, but were not incorporated in most versions of TRIM.SP and TRIDYN. The time dependence of the collision cascade can be chosen as described in [16, 17].

The extensions for SDTrimSP version 5.00 are described. The main new features are the inclusion of diffusion and out-gasing for noble gas ions and chemical erosion of carbon.

## 2. Physical basis

The new program SDTrimSP is based on TRIM.SP [2] and TRIDYN [3, 4]. Both programs, the static TRIM.SP and the dynamic TRIDYN, are described in [1]. The basic physics in the new program SDTrimSP is the same as in the former versions. SDTrimSP is a Monte Carlo program, which assumes an amorphous (randomized) target structure at zero temperature and infinite lateral size.

The target in SDTrimSP is one dimensional (Fig. 1). The target is divided into layers. Y and Z direction are taken as infinite. In the static mode the target is fixed. In the dynamical mode the thickness of layers is changed, [28].

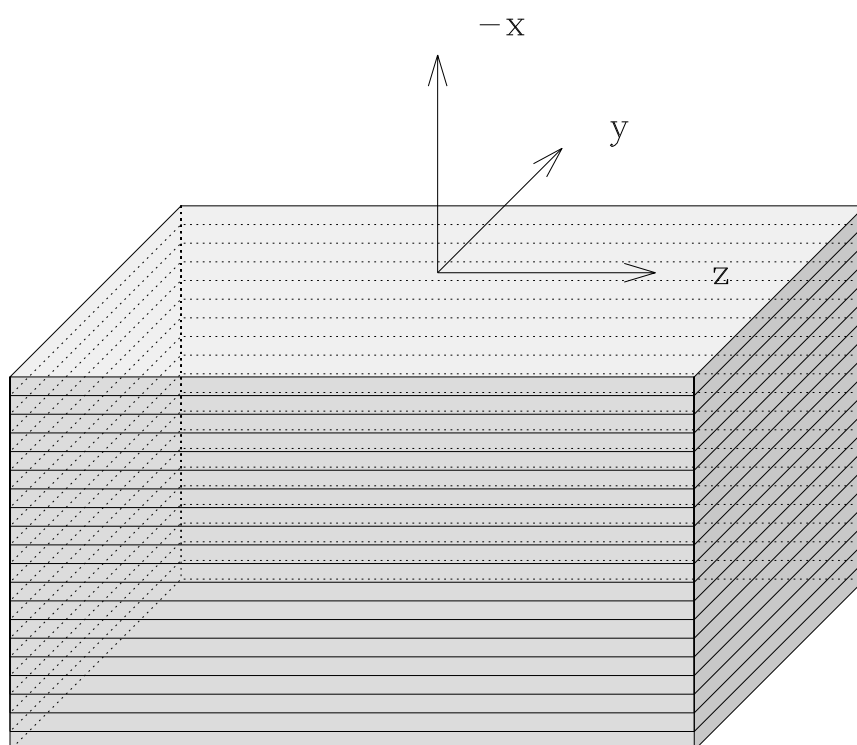


Figure 1: Geometry of the one dimensional target

The binary collision approximation is used to handle the atomic (nuclear) collisions. This means, that the change in flight direction due to the collision is given by the asymptotes of the real trajectory.

For this evaluation an interaction potential has to be chosen (usually purely repulsive and only dependent on the distance between the colliding atoms) to determine the scattering angle of the moving atom and the recoil angle of the atom, which is set into motion. Then the energy loss (nuclear) of the moving atom and the energy gain of the recoil can be calculated. In addition, a moving atom loses energy to target electrons (electronic or inelastic energy loss). The program also provides the possibility to include simultaneous weak collisions, but strictly in the binary collision approximation. The program follows projectiles (incident atoms) and target recoil atoms three-dimensionally until their energy falls below some preset value or if they have left the target (backscattering, transmission, sputtering). Besides a more modular structure many new features are included in the program. Most data needed for a calculation is taken from a database in form of tables: atomic numbers and masses of elements, densities of solid and liquid elements, surface binding energies (heat of sublimation), displacement energies are taken from Table 6.1 of [1]; one table provides isotopic masses of elements; two other tables give the constants for the inelastic energy loss of hydrogen [5] and helium [6]. Different interaction potentials as KrC [7], ZBL [8], Molière [9], Nakagawa-Yamamura [21], power potentials and a special Si-Si potential [10] can be chosen as well as different integration methods of the scattering integral as Magic [11], Gauß-Mehler [12], and Gauß-Legendre [13]. Magic is faster than the Gauß-Mehler and the Gauß-Legendre procedure, but is only available for KrC, ZBL and Molière. Evaluation of the accuracy [14] of the integration procedure Magic shows a maximum relative error of the scattering angle in the center-of-mass system of about 1 % nearly independent of the relative impact parameter (impact parameter/screening length). For the Gauß-Mehler procedure the corresponding error is increasing with an increasing relative impact parameter and depends on the number of pivots [14]. According to Robinson [15], the Gauss-Mehler method is generally more accurate than the Gauss-Legendre method in evaluating the scattering angle integral, but less accurate for the time integral.

### 3. Structure of the code

The code SDTrimSP treats the bombardment of incident ions on different target structures. Besides mono-atomic targets, layer structures, fixed and variable composition target structures are allowed. The kind of projectiles and/or target atoms is not limited. Both incident ions and recoil atoms are treated as series of subsequent collisions. There are two general cases in the code:

- static case: the target composition is fixed during the whole simulation
- dynamic case: modifications of the target caused by the ion bombardment are taken into account; in this case the target is updated at regular intervals, i.e. after a certain number  $NR \geq 1$  of projectiles and corresponding showers. NR has to be specified as a parameter in the input file.

The atoms are distinguished in projectiles (incident atoms) and recoils (target atoms). For each traced atom the important physical quantities, as energy, spatial coordinates,

direction of motion, are recorded along its path using general data structures. Moreover, the path length and the number of collisions are stored for the projectiles, while for the recoils the collision number in which they are generated is stored (generation). Besides the information about the single projectile there are also quantities integrated over all projectiles to save memory. For projectiles, the inelastic (electronic) energy loss and the total elastic and the elastic loss larger than the displacement energy are stored. Other values derived from these basic quantities can be determined, if of interest.

The structure of the program is depicted in Fig. 2. In the projectile loop, groups of NR projectiles are followed from collision to collision. The recoils generated along the projectile trajectories of the NR incident ions are collected and treated in a separate loop, the recoil loop. After finishing the calculation of the NR projectiles and generated recoils the target is updated in the case of the dynamic mode. In the static mode no target update is necessary, and it can be continued with the next group of projectiles until the total number NH of projectiles (number of histories) is reached. Finally, the output section is entered.

In the input file the target and incident particles are specified. A flag determines the static or dynamic mode. In the dynamic case the total fluence for a calculation has to be given in units of  $10^{16}$  atoms/cm<sup>2</sup>. The energy of the incident particles, the angles of incidence, the interaction potential and the inelastic energy loss model have to be chosen. The energy and angle of incidence of the projectile can be chosen fixed or by a given distribution. The input file is organized as a F90 namelist file and described in detail in the documentation delivered with the program package.

The output was designed in a very flexible manner allowing to store all important values of individual particles and offering at the same time the possibility to limit the output in order to save memory and computing time. By conditioning the different output sections in the code the user can switch on or off the different sections with corresponding flags and variables in the input file. Moreover, the output is structured in such a way that the user can insert own output sections in an obvious manner.

The general, obligatory output gives the reflection and sputtering coefficients, atomic fractions and densities as a function of depth, and the yield versus the generation. In the dynamic case the change of target thickness and atomic fractions and densities as a function of fluence is given. This minimal output has a size of some kBytes only. Optional output concerns trajectory information (evolution of spatial coordinates, directions of motion, energy, time), particle information (energy, number of collisions, path length, starting point and final coordinate), matrices (absolute frequency distributions of reflected, transmitted and sputtered particles in discrete levels of energy and exit angles). Note, that the amount of output can increase rapidly to hundreds of MBytes for the trajectory and particle output, especially when the incident energy is high. Especially for problems with a large number of reflected, transmitted and sputtered particles, the usage of matrices output is advantageous as it helps to save memory. There are several post processing programs concerning the matrix output and the visualization of calculated data by means of IDL.



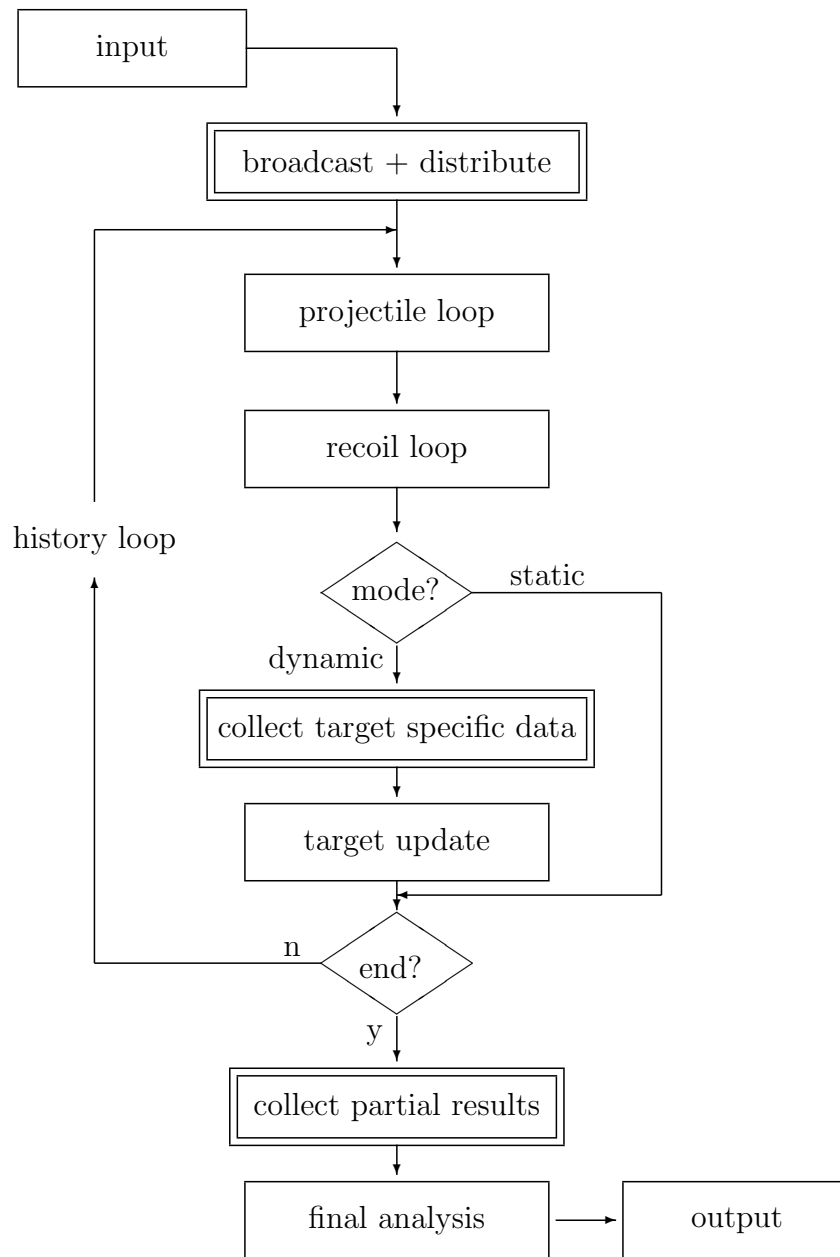


Figure 2: Main block flow chart of the program SDTrimSP. The double blocks indicate additional work necessary in the parallel mode. These parts are skipped in the sequential mode.

## 4. Implementation

The program SDTrimSP is implemented in Fortran 90. The work flow depicted in Fig. 2 is transferred into a modular structure of the code. The characteristic quantities belonging to larger data units like trajectories, particle states and other data blocks are combined in F90 user-defined structures to make data handling easier.

The code is drawn up to work in different modes and on different architectures. Basically, there are two modes:

1. the sequential mode for execution on any sequential architecture with a F90 and a C compiler,
2. the parallel mode for execution on any distributed-memory parallel architecture with a F90 and a C compiler and the MPI communication library available. In this version, the NR particle showers are distributed over the processors.

Both modes are included in the same source code, the different modes are distinguished by use of preprocessor directives. The user selects the mode at compile time by choosing the respective macro in the Makefile.

In the sequential mode the course of the program is as shown in blocks with simple boxes of Fig. 2. In the parallel mode some additional work as specified blocks with double boxes in Fig. 2 is necessary to distribute data structures and computational load and to summarize the results. The parallel algorithm works as follows: The target data is replicated on all processors (broadcast in Fig. 2), while the NR incident ions between two target updates are distributed over  $np$  processors ( $NR \rightarrow NR/np$ ). Furthermore, each processor has to be provided with an appropriate seed for the random number generator (see below). The ions and corresponding showers are simulated independently on the processors, each processor using a dedicated sequence of random numbers. The effects caused by the particles are recorded in processor private variables. This concerns target data, ion specific data and recoil specific data. In the dynamical case, the target data has to be summed up over the processors and made known to each processor in order to perform the target update. The target update is carried out quasi-sequentially on all processors and as a result each processor has a replicate of the new target data and can continue with the next group of ions and so on. In the static case the target update and the global sums are not necessary for the calculation and the summation of the target data is postponed to the end of the program where in any case all particle information gathered locally on the processors has to be collected and printed out. That means the static program is embarrassingly parallel with nearly no communication, while the amount of communication in the dynamic case can be considerable. Depending on the application the computing time may be rather long, therefore restart files can be written at regular time intervals.

The communication is based on the Message Passing Interface (MPI). By this the algorithm is portable between different parallel architectures. Special care has been taken for the generation of random numbers. By choosing the linear congruential random number

generator from Cray's Scientific Library we have a true parallel random number generator having the advantage that the sequence of  $2^{32}$  values can be divided into chunks of equal size so that each processor has its own sequence which is not correlated to the sequences of all other processors. To facilitate debugging and providing reproducible results there is also the possibility to associate each particle with its own, determined seed so that the result of a computation with a certain number of incident particles is always the same irrespective of how many processors are involved. One must, however, be aware that this method of using reproducible random numbers does not yield reliable results in the sense of good statistics. Again, the mode of random number generation is controlled via preprocessor directives in the code and corresponding macros in the Makefile.

The calculation steps in the program SDTrimSP are determined by NR and NH. NR is number of projectiles between target updates, NH is the number of histories. In the dynamic case the target is relaxed after each history step.

Note that the structure of the whole package SDTrimSP is designed in such a way that the same source code, Makefile and run-time commands are used for all modes and architectures and distinctions are made via preprocessor and environment variables (e. g. OSTYPE). The object code is kept in different directories for the different architectures to facilitate the simultaneous usage of different architectures. A detailed description of the code with a list of all input and output variables and a description of all subroutines with references to the corresponding literature is provided. The code is available for free for non-commercial use. (contact mail-address: SDTrimSP@ipp.mpg.de or see the webside: [www.ipp.mpg.de/~stel/SDTrimSP.html](http://www.ipp.mpg.de/~stel/SDTrimSP.html)).

## 5. Performance

The program was tested on several sequential and parallel architectures, as e. g. IBM SP machines, IBM Power4 and Power5 systems, Cray T3E, NEC SX5, and Linux clusters with AMD or Intel processors, and is running in production mode for several years now with great success. For large, time-consuming applications it is advisable to use the parallel version of the code. In this case, the choice of the parameter NR, which is the number of incident particles and corresponding showers between two target updates, is decisive to have good performance, while in the sequential version, this parameter is of no relevance. The reason is that NR is a quantity closely related to the granularity of the parallel algorithm, as each processor has to treat  $NR/np$  incident particles together with their recoils, where  $np$  is the number of processors. That means, NR must not be less than  $np$ , and the larger NR, the better the efficiency of the parallel program, as the ratio between communication and computation decreases. On the other hand, NR has also a physical meaning, as it determines somehow the frequency of target updates. Therefore an investigation of the influence of NR and NH on the accuracy of the results has been carried out.

## 5.1. Influence of NR and NH on the accuracy of the results

A physical interpretation of NR and NH is that a larger number NR improves the statistical relevance of the target update, while a larger number of histories NH means a smaller fluence step (because the fluence step is the total fluence divided by NH) and by this improves the overall statistics. In the static case, the statistics depends only on the product of NR and NH, and NR has no physical meaning.

With the following example of a dynamic case it is shown that the accuracy of the results depends merely on the product of NR and NH over a certain range of values for NR. The chosen example is a 1 keV bombardment of Fe on TaC with a fluence of  $10^{17}$  atoms/cm<sup>2</sup>. The results for different values of NR with  $\text{NR} \cdot \text{NH} = \text{constant}$  are shown in Table 1 and Figs. 3 and 4 at the example of typical quantities. It shows that the plots and values differ only to the same extent as they would differ when using another seed for the random numbers. That means, the number NR may be increased to achieve a better parallel efficiency, while decreasing at the same time the number of histories. For statistical reasons it makes no sense to choose very small values of NH in the dynamic case. The fluence step (total fluence/NH) should be of the order of 0.01 ( $10^{14}$  atoms/cm<sup>2</sup>) to ensure that the target composition change is small in a fluence step.

NR	NH	change of thickness	qu(Fe)	qu(Ta)	qu(C)
1	1000000	4.47 nm	0.559	0.302	0.139
10	100000	4.51 nm	0.557	0.303	0.140
100	10000	4.50 nm	0.557	0.304	0.139
1000	1000	4.49 nm	0.558	0.303	0.139

Table 1: Change of thickness and atomic fraction (qu) of the surface composition with different numbers of NR and NH for the example of Fe  $\rightarrow$  TaC ( $\text{NR} \cdot \text{NH} = \text{constant}$ )

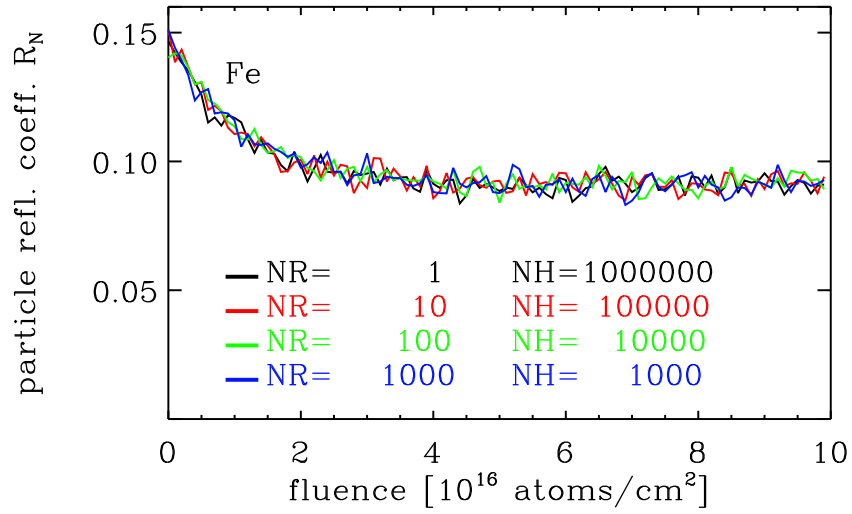


Figure 3: Particle reflection coefficient for different numbers of NR and NH ( $\text{NR} \cdot \text{NH} = \text{constant}$ ) in the case of 1 keV Fe atoms impinging at normal incidence onto a TaC target

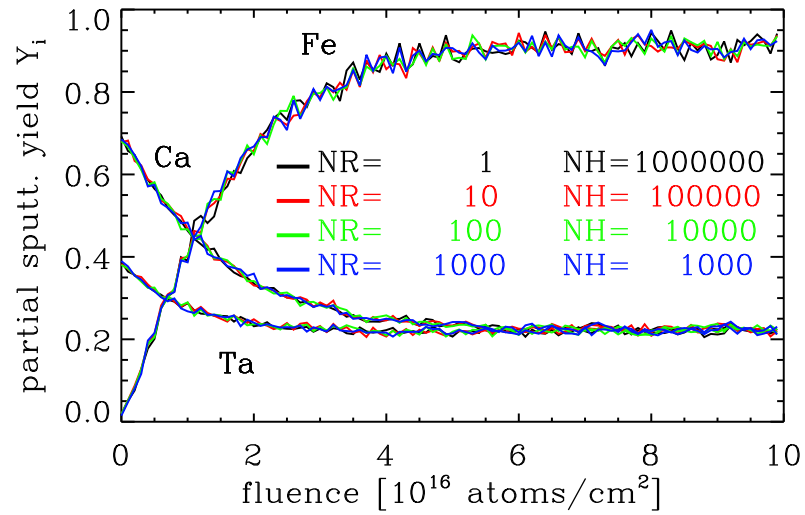


Figure 4: Partial sputtering yield for different numbers of NR and NH ( $\text{NR} \cdot \text{NH} = \text{constant}$ ) in the case of 1 keV Fe atoms impinging at normal incidence onto a TaC target

## 5.2. Parallel efficiency

As already pointed out the performance of the program depends strongly on the mode and on the choice of NR on the one hand, but on the other hand on the characteristics of the used architecture. When working on a single-processor system, i.e. using the sequential version, it is mainly the clock rate of the processor which determines the computing time, irrespective of whether using the static or dynamic mode. The choice of NR is not of great importance. In the dynamic case, however, the code is rather communication-intensive, and the performance depends heavily on the choice of NR.

These dependencies are demonstrated at the example of 1 keV Fe bombardment on TaC at normal incidence with a fluence of  $10^{16}$  atoms/cm<sup>2</sup>. The benchmark has been carried out on two different parallel architectures, an IBM 1.3-GHz-Power4 (Regatta) system and a Linux cluster with Intel 2.8-GHz processors. The Regatta system is provided with a fast communication network with Federation switch, while the nodes of the Linux cluster are connected via Gigabit Ethernet. For these benchmarks the option of minimum output was used, the parameters NR and NH have been chosen as NR = 512 and NH = 20000 which allows to use up to 512 processors in the parallel mode.

The execution times and parallel efficiencies obtained for the static mode on the two architectures are shown in Table 2. As expected the parallel efficiency of the code is very good on both architectures, because the amount of communication is very low and consists mainly in broadcasting the data at the beginning of the calculation and summing up the partial results of the processors at the end of the calculation. This is also reflected in the corresponding speedup curves, cf. the solid lines in Fig. 5(b).

Table 3 and the dashed lines in Fig. 5(b) show the corresponding behavior for the dynamic case. There is a clear difference in the performance for the two architectures. The parallel efficiency obtained with the IBM Regatta is very good up to 64 processors. This is due to the fast communication achieved by the strong Federation switch of the Regatta system and the MPI implementation on top of the shared memory architecture of the Regatta. In contrast, the parallel efficiency on the Linux cluster is not that good. This is due to the fact that the communication network of the Linux cluster is rather slow compared to the processor performance and cannot cope with the amount of communication. The speedup curves demonstrate the somewhat poorer scaling and show that the Linux cluster is not specially suited for parallel calculations with more than 16 processors in the dynamic mode. Up to 16 processors, however, the performance of the Linux cluster is quite satisfactory, at least for the chosen value of NR = 512. It should be noted that the single-processor performance of the Linux cluster is much better than that of the IBM Regatta.

To conclude, the mode of the calculation, the choice of different parameters and the characteristics of the parallel architecture determine the efficiency of the calculation. To improve the performance in the dynamic mode it is advisable to reduce the communication by using a small number of NH and a large number of NR.

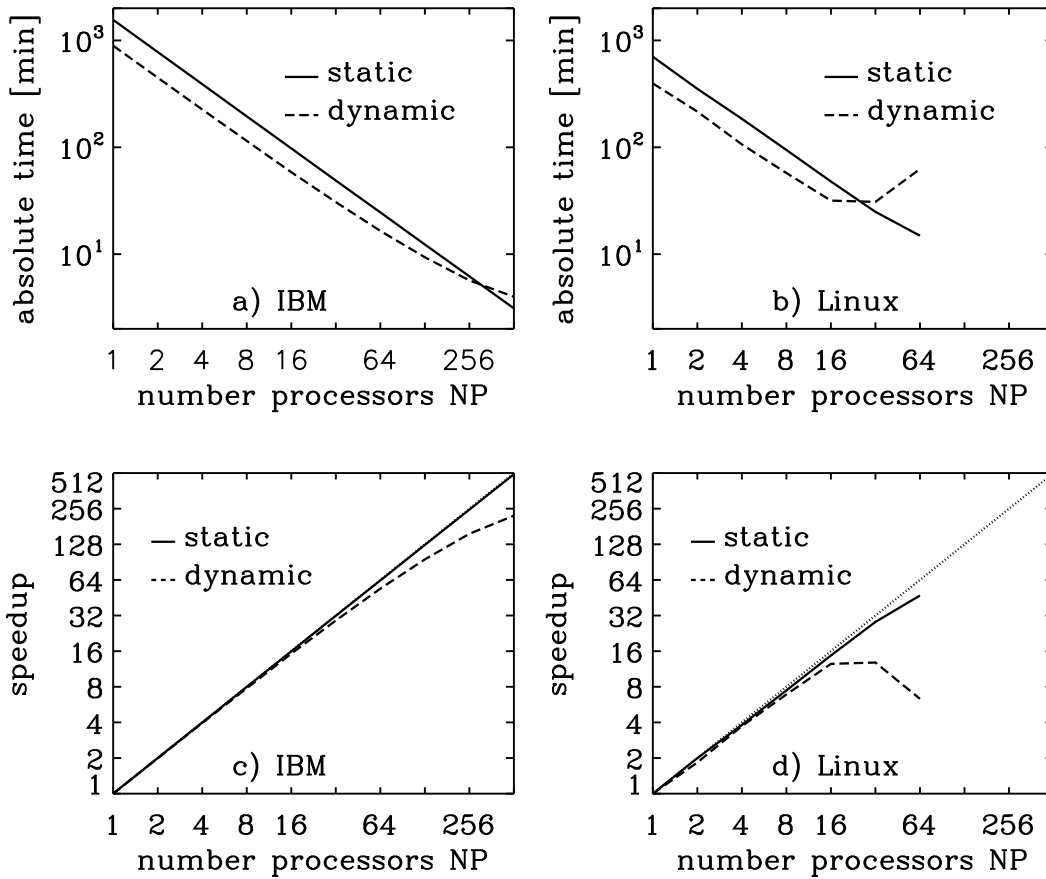


Figure 5: a, b) Absolute time and c, d) speedup of the static and dynamic cases in dependence of the number of processors for the IBM Regatta (IBM) and an Intel Linux cluster (Linux)

$np$	IBM Regatta 1.3 GHz		Linux cluster 2.8 GHz (Intel)	
	execution time [min]	parallel efficiency	execution time [min]	parallel efficiency
1	1557.38	1.000	703.84	1.000
2	778.61	1.000	352.47	0.998
4	389.96	0.998	184.78	0.952
8	194.81	0.999	94.40	0.931
16	97.65	0.996	47.86	0.919
32	48.87	0.995	24.90	0.883
64	24.86	0.989	14.89	0.738
128	12.31	0.988		
256	6.20	0.981		
512	3.11	0.978		

Table 2: Execution time and parallel efficiency of the static version of SDTrimSP on the IBM Regatta and on an Intel Linux cluster for the example of 1 keV Fe atoms impinging at normal incidence onto TaC with NR = 512, NH = 20000 (10240000 particles)

$np$	IBM Regatta 1.3 GHz		Linux cluster 2.8 GHz (Intel)	
	execution time [min]	parallel efficiency	execution time [min]	parallel efficiency
1	891.90	1.000	395.90	1.000
2	448.17	0.995	215.72	0.917
4	225.84	0.987	106.48	0.929
8	114.77	0.971	57.46	0.861
16	58.47	0.953	31.69	0.780
32	30.72	0.907	30.85	0.401
64	16.51	0.844	62.58	0.098
128	9.35	0.745		
256	5.68	0.613		
512	3.99	0.436		

Table 3: Execution time and parallel efficiency of the dynamic version of SDTrimSP on the IBM Regatta and on an Intel Linux cluster for the example of 1 keV Fe atoms impinging at normal incidence onto TaC with NR = 512, NH = 20000 particles



## 6. Special applications

### 6.1. Static mode

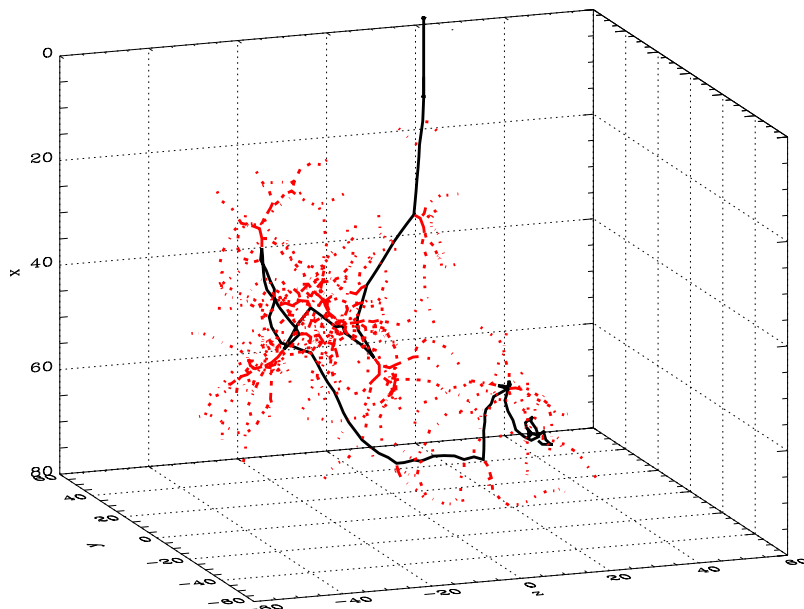


Figure 6: Trajectory of a 2 keV He atom penetrating a Ni target at normal incidence. The color indicates the projectile (black) and the recoils (red).

**Trajectories** A typical trajectory of a 2 keV He atom in a mono-atomic Ni target is shown, see Fig. 6. The path of the incident He atom, the projectile, is black and the paths of all recoils are red.

The decreasing energy of the atom along its path through the solid is indicated by the color, Fig. 7(a). The atom is stopped if its energy is smaller than the cutoff energy which is chosen to be 1.0 eV. In Fig. 7(b) the same trajectory as in the preceding figure is shown together with the generated Ni recoils. The recoils of the first generation are indicated in red, the recoils of the second generation in blue.

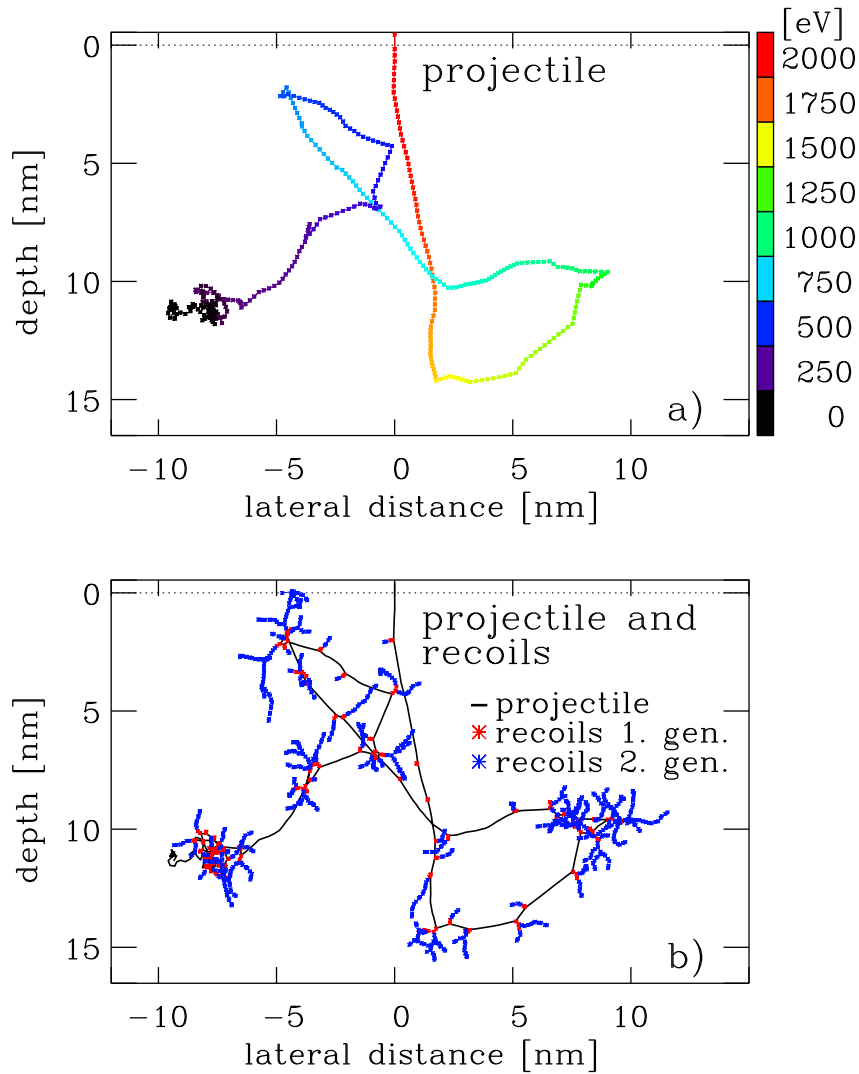


Figure 7: Trajectory of a 2 keV He atom penetrating a Ni target at normal incidence. a) The color indicates the decreasing energy of the He atom along its trajectory. b) In addition to the He trajectory also the generated recoils are shown. The color indicates the recoils of first generation (red) and the recoils of the second generation (blue).

**Angular distribution of scattered and sputtered atoms** Here, we consider the bombardment of an Ni target with 1 keV Ar at  $60^\circ$ . The contour plots for the angular distributions of the reflection coefficient and of the yield per solid angle are shown in Fig. 8. The largest coefficient for the backscattered particles is reached in the forward direction at a polar angle of about  $75^\circ$ , whereas for the backscattered atoms a high-intensity ridge appears in the forward direction up to an azimuthal angle of  $40^\circ$ . The highest yield per solid angle occurs in the forward direction at about  $30^\circ$ . The lowest coefficients are in the backward direction for both kinds of particles.

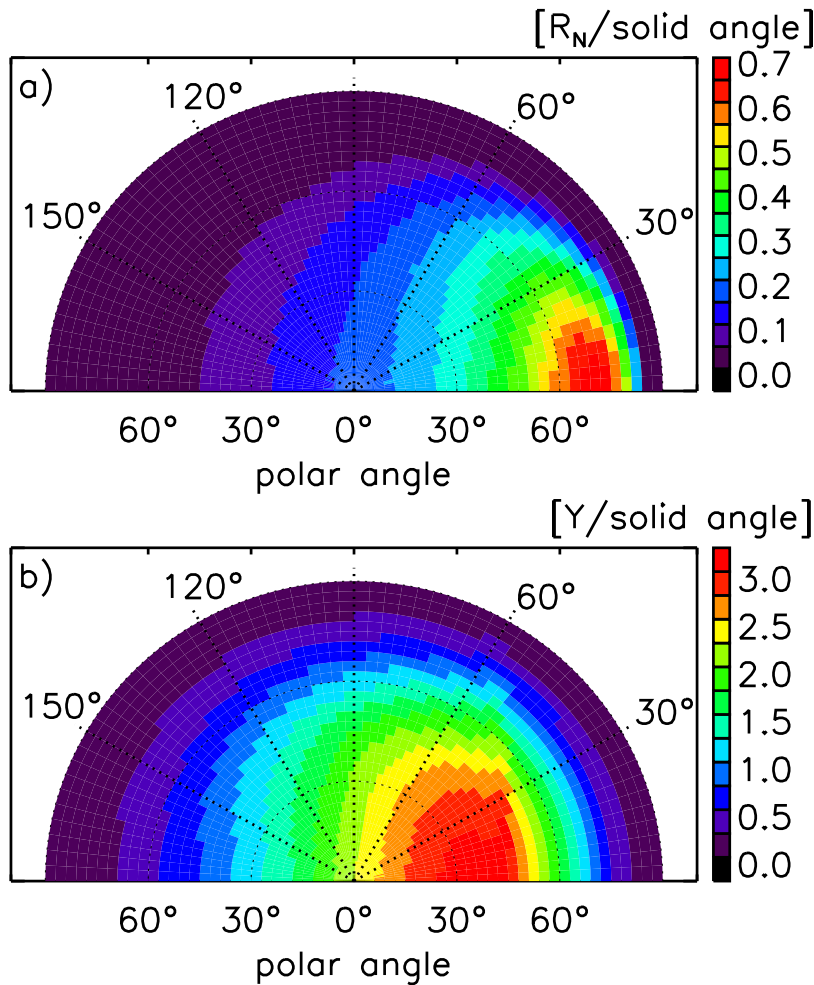


Figure 8: Contour plot of the angular distribution of the coefficient per solid angle of a) backscattered Ar atoms and b) sputtered Ni atoms. A Ni target is bombarded with  $10^8$  1 keV Ar atoms at  $60^\circ$ . The intensity is indicated by the color.

## 6.2. Dynamic mode

**Backscattering coefficient, sputtering yield and atomic fraction** Fig. 9 shows the fluence dependence of the particle backscattering coefficient,  $R_N$ , and the partial sputtering yields,  $Y_i$ , for the bombardment of the compound target WC with 10 keV Ni at normal incidence. At a fluence of about  $10^{17}$  atoms/cm<sup>2</sup>  $R_N$  and  $Y_i$  become constant, which means that steady state or equilibrium is reached. The backscattering coefficient of Ni is decreasing with increasing fluence because some of the heavy W atoms are replaced by the lighter Ni atoms. This can be seen in Fig. 10, where the atomic fractions of the three species are shown versus depth at different fluences. The partial yield of Ni is increasing from zero (pure WC target) to a constant value. At steady state the amount of Ni in the target is not changing any more with fluence which means that  $R_N + Y_{Ni}$  must be unity. It can also be noted from Fig. 10, that the depletion of C in the target is larger than that of W. It is a well-known fact, that in many cases the lighter element in a multi-component target is preferentially sputtered. It should be remembered that diffusion and segregation effects are not included in the calculations.

**Dynamic changes of the target composition** Another interesting case is the bombardment of a target consisting of light atoms by heavy ions, in this case the bombardment of C by W at normal incidence. At the beginning of the bombardment, the target swells (positive value of surface position). This is a result of the deposition of W into the carbon target, which is larger than the sputtering of C. The composition of the target is changed particularly after a fluence of  $5 \cdot 10^{16}$  atoms/cm<sup>2</sup>. Therefore, the sputtering and reflection of W starts and the target shrinks (negative value of surface position), see Fig. 11(a). The values of backscattering and sputtering change quasi-periodically according to the composition of the target, see Fig. 11(d). The peak of the partial yield of W ( $Y_{Si}$ ) appears when the peak of the W implantation profile reaches the surface; the self-sputtering of W is much larger than the sputtering of C by W. The occurrence of further peaks is caused by the generation of further implantation profiles of W until they die out. After a fluence of  $30 \cdot 10^{16}$  atoms/cm<sup>2</sup> a static state or equilibrium is reached and the coefficients  $R_N$  and  $Y_i$  get constant, see Fig. 11(b,c).

**Target composition** The program allows also layered target structures. As an example a target with several Si and Ta layers on Si is chosen, which is bombarded at normal incidence with 3 keV Ar. The oscillatory behavior of  $R_N$  and  $Y_i$  originates from the layered structure. For  $R_N$  the reason for the maxima is the higher reflection coefficient of Ar from Ta compared to that from Si due to the different mass ratio of target atom to incident ion. The peak of  $Y_{Si}$  at a fluence of about  $5 \cdot 10^{17}$  atoms/cm<sup>2</sup> originates from the higher backscattering of Ar from the underlying Ta. Fig. 12 shows the broadening of the depth profile, the atomic mixing and the recoil implantation in the target. Again, in this example the lighter target element, Si, is preferentially sputtered. In this run, the implantation of Ar into the target is neglected.

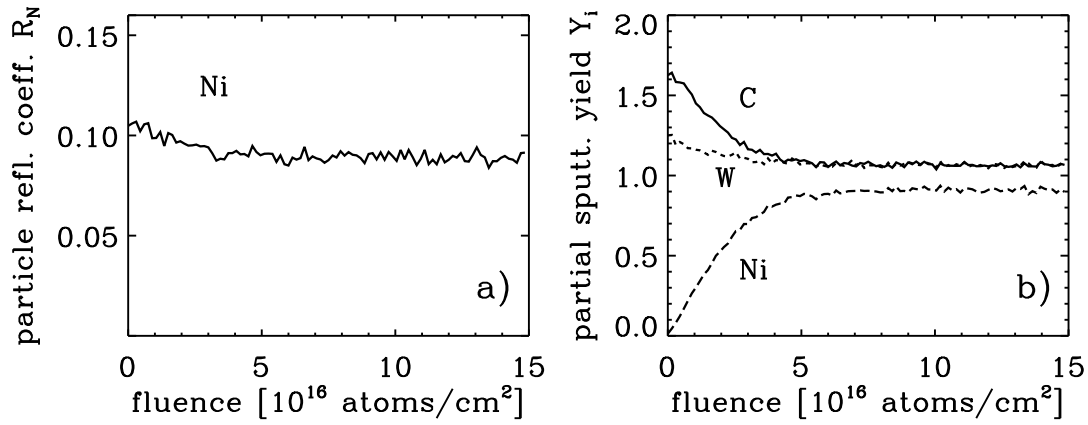


Figure 9: Fluence dependence of a) the particle reflection coefficient,  $R_N$ , and b) the partial sputtering yields,  $Y_i$ , by Ni on WC at normal incidence. A WC target is bombarded with 10 keV Ni.

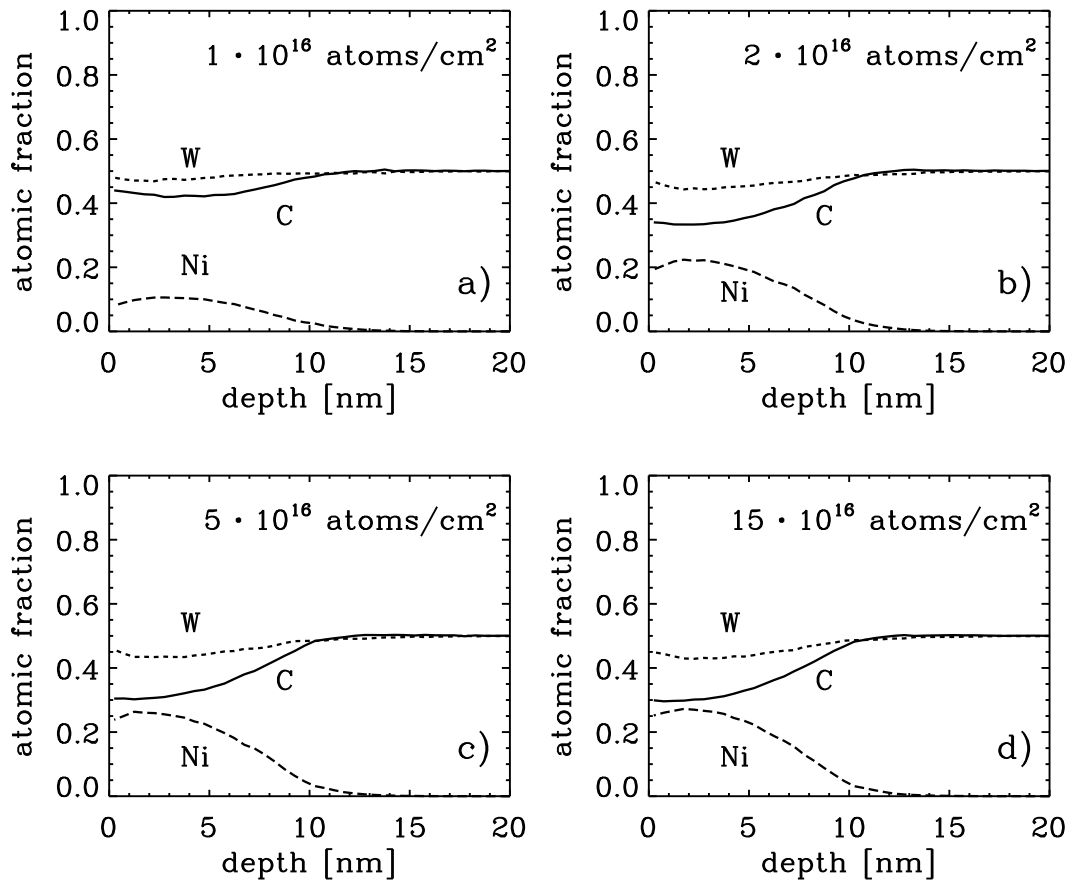


Figure 10: Atomic fraction of C, Ni and W versus depth dependent on fluence. A WC target is bombarded with 10 keV Ni at normal incidence.

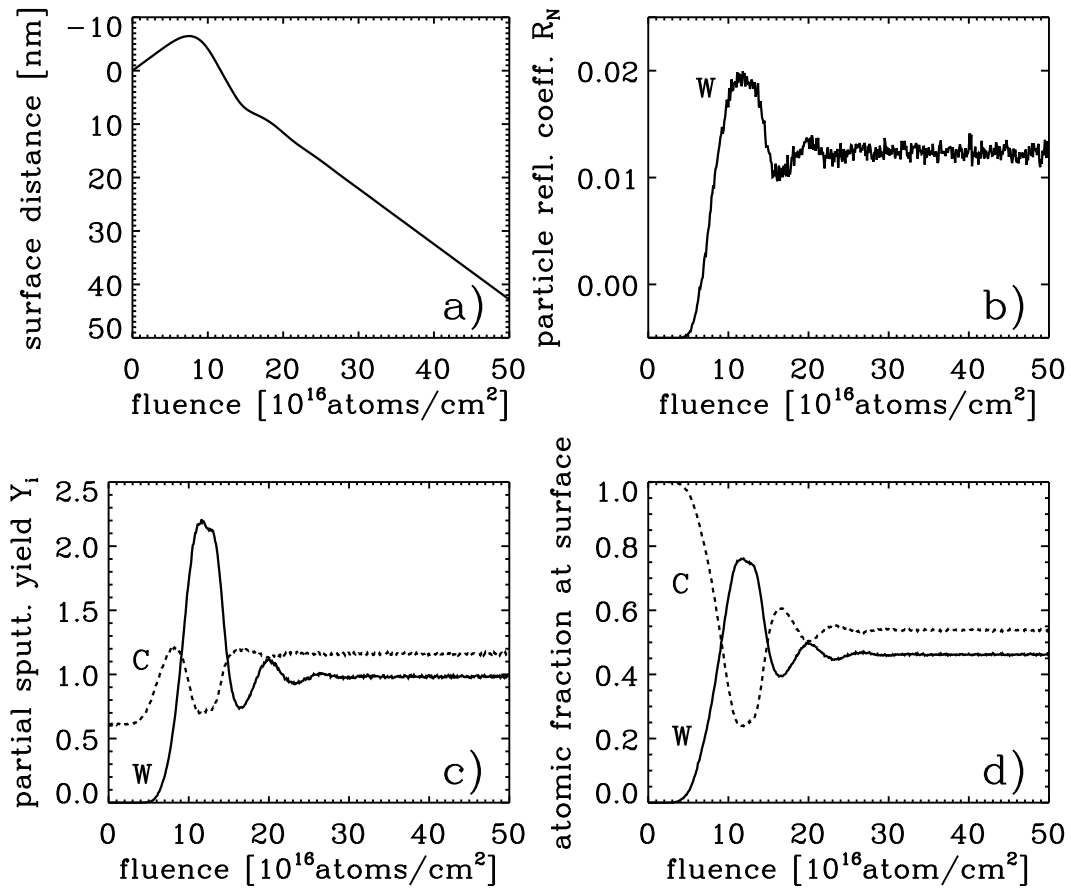


Figure 11: a) Surface distance, b) Particle reflection coefficient,  $R_N$ , of W, c) partial sputtering yields,  $Y_i$ , of C and W and d) atomic fractions of W and C for the bombardment of a C target at normal incidence with 5 keV W atoms.

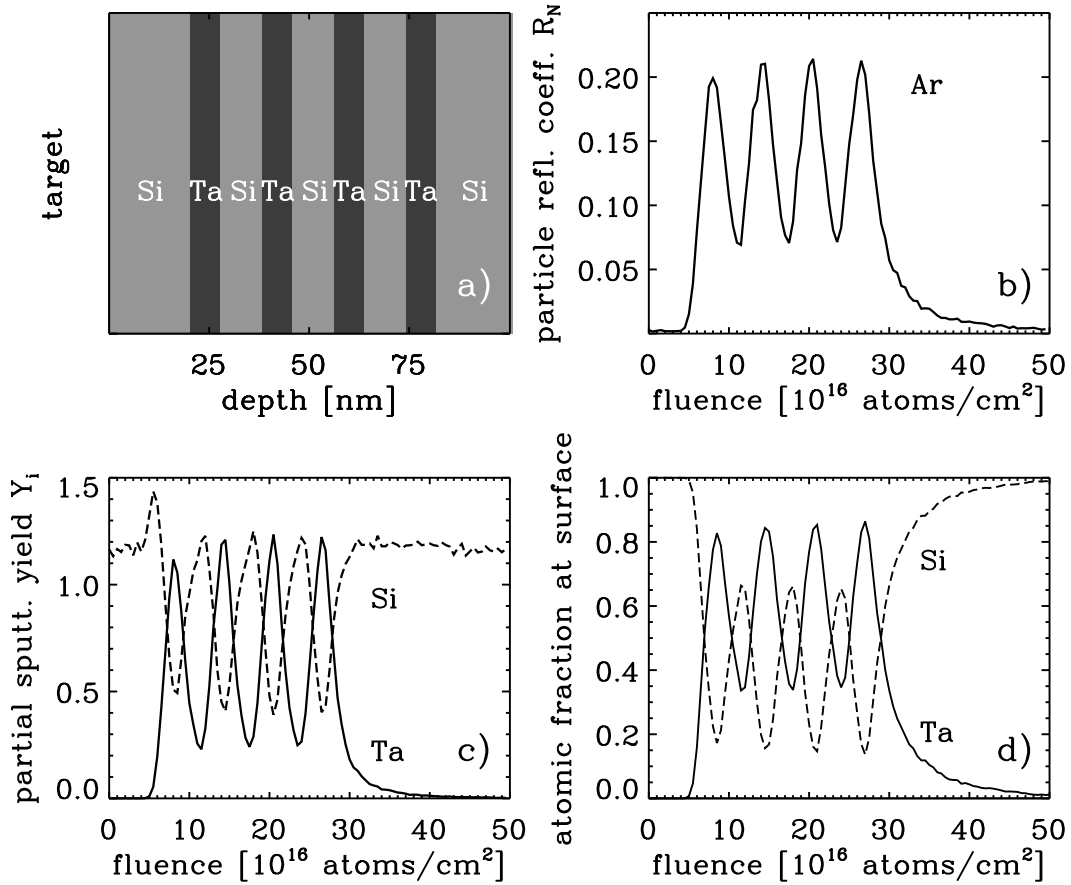


Figure 12: A Si(20 nm)[Ta(7.5 nm)Si(10.5 nm)]<sub>3</sub>Ta(7.5 nm)Si target is bombarded by 3 keV Ar at normal incidence. a) Initial target composition, fluence dependence of b) the particle reflection coefficient,  $R_N$ , c) the partial sputtering yields,  $Y_i$  and d) the atomic fraction of Si and Ta at the surface (depth 0 - 0.5 nm).

## 7. Extension in Version 5.00

### 7.1. Sputtering with noble gas ions

The implantation of gas atoms in the target changes the density and the scattering behaviour inside the solid and has, therefore, an influence on the collision cascade, on the depth profile and on sputtering. Due to the low binding energy of gas atoms (nearly zero for noble gases) they can get more easily sputtered. Therefore, the gas concentration near the surface is lower than in deeper layers. Another effect of the low binding energy is the possible out-gasing of noble gas atoms.

The description of the escape of noble gas atoms from the target in the TRIM [1] and SDTrimSP (version less than 4.14) [27] is inadequate. The effect of out-gasing in these programs was realised by the re-emission of gas atoms, namely the removal of atoms from the target without any transport of these atoms through the surface. In this case the knowledge of the maximum atomic fraction of the noble gas content in the solid is required for their removal.

This introduction of an upper limit for the concentration of gas atoms, which must not be exceeded, does not describe the process itself and does not calculate profiles of gas atoms in the target, corresponding to the physical correct situation.

A first attempt to describe the out-gasing in the SDTrimSP using a gas transport model [23] gives very good agreement of the fluence-dependent areal density values for energy larger than 10 keV.

However, as shown in [24], the maximum of the atomic fraction as a function of the energy of the incident atoms and the stationary profiles of Xe are not reproduced correctly. Also a physical explanation of a constant gas transport is difficult to provide.

To develop a model that reproduce the steady-state profiles, areal density values and maxima of the atomic fraction, the following assumptions are used:

1. The implanted gas atoms can not diffuse independently. The measured profiles [25] after the bombardment of Xe on Si are the same as those produced during the bombardment.
2. During the bombardment the implanted gas atoms lead to a swelling of the target, so that a pressure arises, which is only gradually removed through relaxation. This pressure is described by the difference in concentration of the gas atoms (similar to the diffusion pressure) in the target  $dn/dx$ .
3. The implanted gas atoms are not bounded in the target. They can only move into the direction of the surface if a pressure gradient exists and the atoms get an external excitation. This excitation can be caused by atomic damages during the collisional cascade. The collisional cascade and therefore also the atomic damages start at the surface and end deep in the target. Therefore, movement of gas atoms is only possible in the direction of the surface. The transport of gas atoms can appear only within the range of the depth of penetration and a diffusive flux into the interior of the target can therefore not take place.



According to Fick's diffusion law the flux  $J$  is:

$$J = -D \cdot \frac{\partial n}{\partial x} \quad (7.1)$$

$D$  is the diffusion coefficient,  $n$  is the concentration (number density) and  $x$  is the depth.

This gives for the fluence  $\Phi$ :

$$\frac{\partial n}{\partial \Phi} = -\frac{\partial(D \cdot \frac{\partial n}{\partial x})}{\partial x} \quad (7.2)$$

The diffusion coefficient depends on energy  $E$ , the gradient  $\partial n/\partial x$  and the atomic fraction  $q$ :

$$D = f\left(\frac{\partial n}{\partial x}, q, E\right) \quad (7.3)$$

If the gradient  $\partial n/\partial x$  is negative than the diffusion coefficient is zero.

$$D = 0 \quad \frac{\partial n}{\partial x} \leq 0 \quad (7.4)$$

If the gradient is positive the diffusion coefficient is:

$$D = D_0 \cdot D_1(q, x, E) \quad \frac{\partial n}{\partial x} > 0 \quad (7.5)$$

$D_0$  is a constant value.

$D_1$  is variable and dependent on atomic fraction  $q$  and the relative number atomic damages  $dam$  of gas. The maximum of  $q$  and  $dam$  is one. The number atomic damages in the target is dependent on energy  $E$  and depth  $x$  at each fluence step.

$$D_1(q, x, E) = dam(E, x) \cdot (1.0 - e^{-q(x)}) \quad (7.6)$$

The relative number of damages is the ratio of absolute number of damages  $N_{dam}$  and their maximum.

$$dam(E, x) = \frac{N_{dam}(x)}{max(N_{dam}(x))} \quad (7.7)$$

The larger the relative number of damages  $dam$  and the concentration of gas  $q$ , the larger the diffusion-coefficient  $D$ . The influence of  $q$  is non-linear.

This diffusion is also dependent on energy the of the incident particle.

## Results

The diffusion coefficient  $D_0$  was determined so that the experimental profile of the atoms fraction of Xe for an energy of 40eV are reproduced, Fig. 15.

$$\begin{aligned} D_0(Xe) &= 2.8 \cdot 10^6 \text{ \AA}^4/ion \\ D_0(Xe) &= 2.8 \cdot 10^{-34} \text{ m}^4/ion \end{aligned} \quad (7.8)$$

for Ar the diffusion coefficient  $D_0$  is:

$$\begin{aligned} D_0(\text{Ar}) &= 1.9 \cdot 10^5 \text{ \AA}^4/\text{ion} \\ D_0(\text{Ar}) &= 1.9 \cdot 10^{-35} \text{ m}^4/\text{ion} \end{aligned} \tag{7.9}$$

The measured depth profiles, see Fig. 13, is difficult to reproduce. A gradient must be present to ensure a steady flow. The dashed line shows the diffusion coefficient  $D_1$ . The area density Fig. 14 and maximum atomic fraction Fig. 15 in dependency of the energy are reproduced well.

The results for the areal density of Xe are shown in Fig. 16. The agreement with the measurement [26] is very good.

The development of the profile of Xe with an incident energy of 145 keV is shown in Fig. 17 fitting well the measurement.

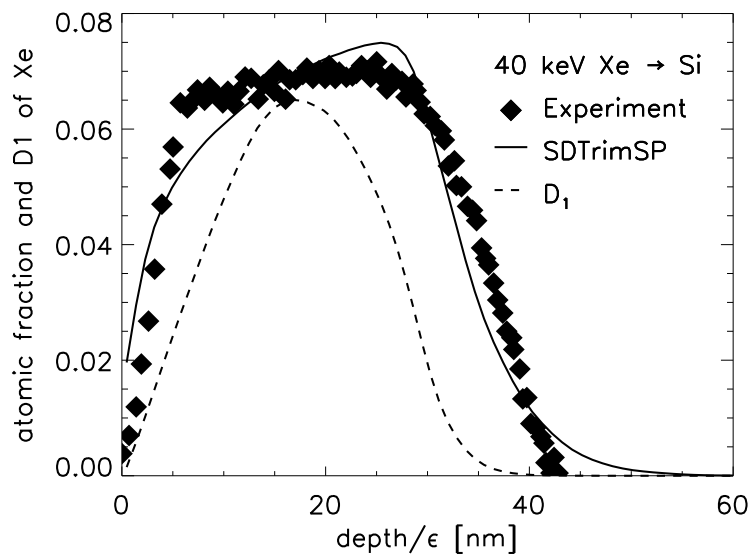


Figure 13: Calculated depth profiles of the implanted Xe 40 keV xenon in silicon compared with experimental data [25] and diffusion-coefficient  $D_1$ .

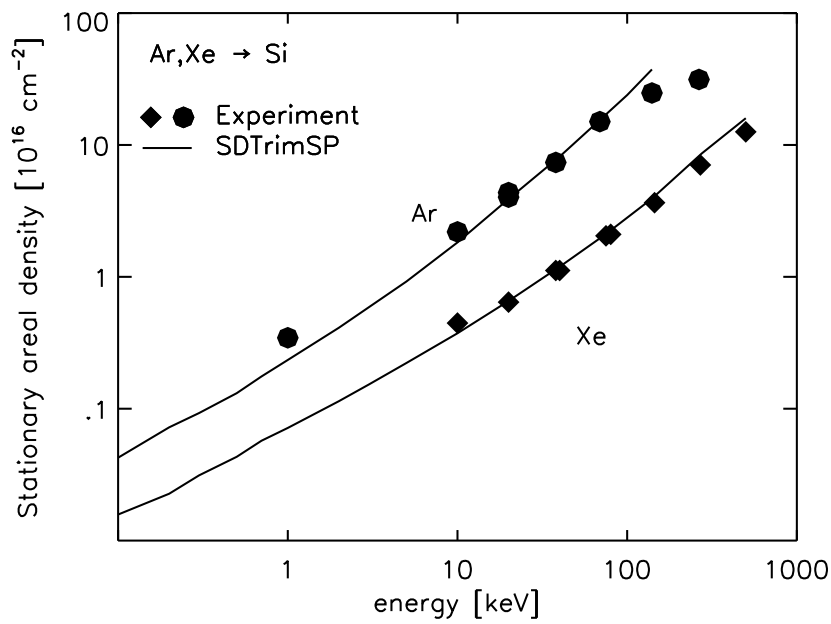


Figure 14: Calculated steady state areal density of implanted Xe versus the incident energy of Xe on a Si target at normal incidence compared with experimental data [24]

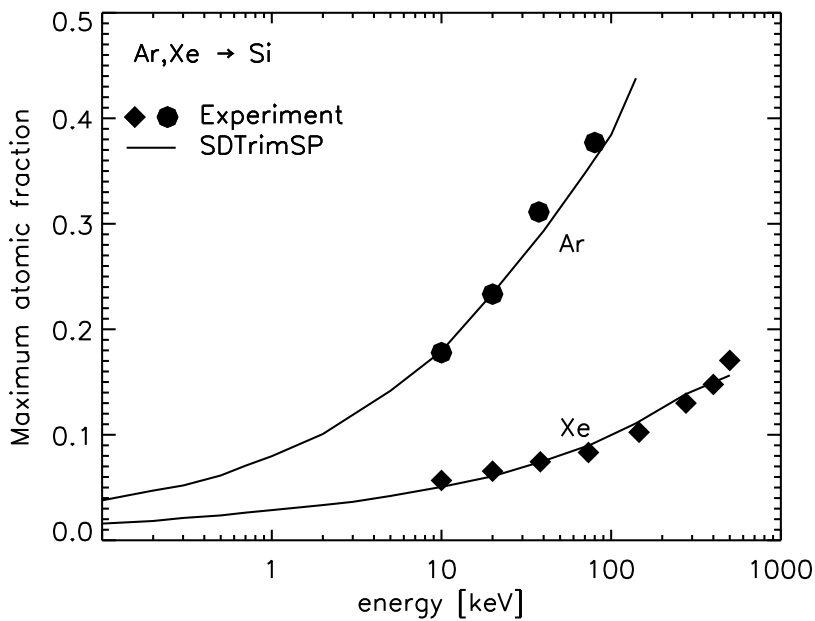


Figure 15: Calculated steady state maximum atomic fraction of implanted Xe versus the incident energy of Xe on a Si target at normal incidence compared with experimental data [24]

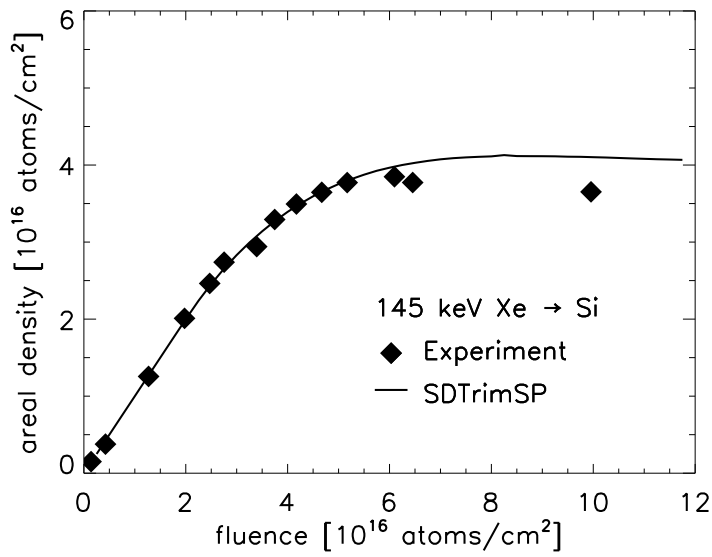


Figure 16: Calculated areal density of implanted Xe versus the incident fluence compared with experimental data [26]. Si is bombarded with 145 keV Xe at normal incidence

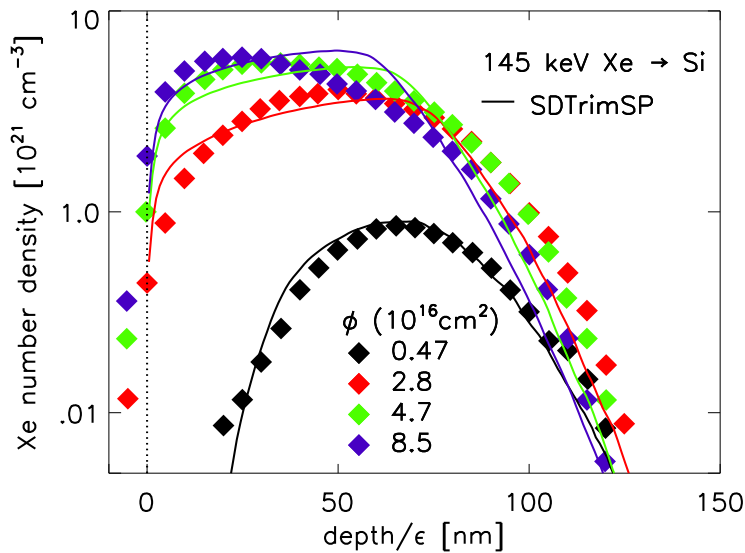


Figure 17: Calculated profile of implanted Xe compared with experimental data [26]. Si is bombarded with 145 keV Xe at normal incidence

## 7.2. Chemical erosion of carbon

The total methane erosion yield ( $Y_{CH_4}$ ) is calculated as a sum of a kinetic contribution  $Y_0$  at  $T_0 = 300K$  and of a temperature dependent or thermal contribution  $Y_T$ , [32].

$$Y_{CH_4} = Y_0(E, T_0, sp^3, sp_{CH}^x) + Y_T(E, T, sp^3, sp_{CH}^x) \quad (7.10)$$

$E$  is the energy of incident particles.  $sp^3$  and  $sp_{CH}^x$  are carbon hybridization states.

### Introduction of different carbon hybridization states

In the version of SDTrimSP without chemical erosion carbon atoms were simulated as a single species, C\_g. For simulating chemical erosion one needs to distinguish carbon atoms having different hybridization states as different species. Therefore, the chemistry module describes an a-C:H film in terms of three carbon species namely,  $sp^2$  (carbon with double bonds),  $sp^3$  (carbon with single bonds and not bonded to H atom) and  $sp_H^3$  ( $sp^3$  carbon with a bonded H atom). The code has been modified to include the following chemical reactions:

1. If an impinging ion transfers more than a critical value of energy,  $e_{displ} = 3.75$  eV, to a  $sp^2$  carbon then the double bond is broken and a  $sp^3$  carbon is created.
2. Since there is an upper limit of 1/3 on H atoms bonded to C for typical C:H film, this was used as a limit, *i. e.*,
  - if the concentration of H ( $n_H$ ) or  $sp^3$  ( $n_{sp^3}$ ) exceeds the concentration of  $sp_H^3$  ( $n_{sp_H^3}$ ),  $sp^3$  carbon is changed to  $sp_H^3$ .
  - if  $n_H$  or  $n_{sp^3}$  is less than  $n_{sp_H^3}$ ,  $sp_H^3$  is transferred to  $sp^3$ .
3. The maximum concentration of carbon centers in  $sp^3$  hybridization state ( $sp^3$ ,  $sp_H^3$ ) is controlled (as a feedback mechanism) from the values calculated by the Mech model [31] ( $sp^3, sp_H^3, sp_{CH}^3$ ) and is dependent on temperature. For example, at a given temperature, if the total concentration of carbon centers in  $sp^3$  hybridization state calculated from SDTrimSP ( $n_{sp^3} + n_{sp_H^3}$ ) is greater than the corresponding value predicted by the Mech model, then  $sp_H^3$  will change into  $sp^2$  carbon.

### Contribution from the kinetic part

The calculation of the kinetic part,  $Y_0(E, T_0)$ , of the erosion yield is based on the mechanism proposed by Hopf [30]. Lets say  $Y_{BB}$  represents the number of bond breaking of  $sp_H^3$  caused by an impinging ion and  $Y_{Hstop}$  gives the yield of the H atom implantation. This stopped or implanted H atoms can be bonded to free open carbon bonds.

For hydrocarbon formation both open carbon bonds and hydrogen atoms must be available. In order to include this effect the minimum of  $Y_{BB}$  and  $Y_{Hstop}$  is taken. For an out-diffusion probability of a hydrocarbon molecule from a depth  $x$  the kinetic part of the chemical erosion yield  $Y_0(E, T_0)$  is given by

$$Y_0(E, T_0) = \int_0^d a \cdot \min[Y_{BB}, Y_{Hstop}] \cdot e^{(-x/\lambda)} dx \quad (7.11)$$

Here,  $\lambda$  ( $= 0.4$  nm) is the typical range of out-diffusion for hydrocarbon and  $d$  is the depth of the sample. If the whole sample is divided into  $k$  strips or depth intervals parallel to the surface as in SDTrimSP

$$Y_0(E, T_0) = \sum_0^k a \cdot \min[Y_{BB}(k), Y_{H_{stop}}(k)] \cdot e^{(-x(k)/\lambda)}. \quad (7.12)$$

The minimum condition  $\min[Y_{BB}(k), Y_{H_{stop}}(k)]$  expresses the fact that chemical erosion only happens when sufficient open bonds ( $Y_{BB}(k)$ ) and sufficient hydrogen ( $Y_{H_{stop}}(k)$ ) are available. Therefore, the minimum of both will limit the production of hydrocarbons. The value of the coefficient  $a$  range from 0.04 to 1.0 and was obtained by the comparison between measurements and simulation results.

$$a = \min[1.0, 0.04 + 0.01 \cdot \frac{Y_{H_{stop}}(k)}{Y_{BB}(k)}] \quad (7.13)$$

### Contribution from the thermal part

The temperature dependent part of the chemical erosion yield,  $Y_T(E, T, \Phi_0)$ , in the code is based on the Mech model [31].

$$Y_{TMech}(E, T, \Phi_0) = \rho \cdot sp_{CH}^x \frac{Ex}{\Phi} \quad (7.14)$$

$\rho$  is the surface density of carbon atoms:  $\rho = 6.0 \cdot 10^{19}$  atoms/m<sup>2</sup>.

$$Y_T(E, T, \Phi_0) = \sum_1^n \frac{Y_{T-Mech}(E, T, \Phi_0)}{sp^3 + sp_{CH}^x} \cdot e^{(-x/\lambda)}. \quad (7.15)$$

Here  $n$  is the total number of collisions between ions and  $sp_H^3$ . The depth dependent out-diffusion probability after the hydrocarbon formation  $e^{(-x/\lambda)}$  is added. The term  $Y_{T-Mech}(E, T, \Phi_0)$  is the yield of chemical erosion at a constant flux of ( $\Phi_0 = 10^{18}$  m<sup>-2</sup>s<sup>-1</sup>).

### Flux dependence of chemical erosion

It is observed that the kinetic part of the erosion yield is flux independent, therefore, in order to implement the correct flux dependence the thermal contribution ( $Y_{therm}$ ) to the erosion has to be flux dependent. A flux interpolation is done with the help of Roth's formula [29].

The erosion yield given by the Mech model is correct only for a flux of  $10^{18}$  m<sup>-2</sup>s<sup>-1</sup> (this is kept as the reference level flux  $\Phi_0$ ). It has been observed that with increasing flux, the temperature at which the yield is maximum ( $T_{max}(E, \Phi)$ ) and the absolute value of the yield ( $Y_{max}(E, \Phi)$ ) increases. It is assumed that  $T_{max}(E, \Phi)$  predicted by the Roth model is correct (although  $Y_{max}(E, \Phi)$  is not). Then in order to calculate the flux dependent erosion yield for a given flux  $\Phi$  and energy  $E$ , one proceeds as follows:

1. First the  $\Delta T$  from Roth's formula (see Fig. 18) is computed

$$\Delta T = T_{max}(E, \Phi) - T_{max}(E, \Phi_0) \quad (7.16)$$

2. then the erosion yield from the Mech model at  $T - \Delta T, \Phi_0$  is calculated

$$Y_{T\_Mech}(E, T - \Delta T, \Phi_0) \quad (7.17)$$

3. the corrected flux dependent erosion yield is given by

$$Y_{Tcor}(E, T, \Phi) = Y_{T\_Mech}(E, T - \Delta T, \Phi_0) \cdot \frac{Y_{Roth}(E, T, \Phi)}{Y_{Roth}(E, T, \Phi_0)} \quad (7.18)$$

If the sample is composed of  $n$  layers, then the total flux dependent thermal erosion yield is

$$Y_T(E, T, \Phi) = \sum_1^n \frac{Y_{Tcor}(E, T, \Phi)}{sp^3 + sp_{CH}^x} \cdot e^{(-x/\lambda)} \quad (7.19)$$

Finally the total erosion yield of carbon is:

$$Y = Y_{physical}(E) + Y_0(E, T_0) + Y_T(E, T, \Phi) \quad (7.20)$$

In the following part of this section the general algorithm in the simulation and its technical implementation is presented, [32].

A pre-calculated number of energetic particles, depending on the fluence, are incident on the target. The target is divided into 1D layers and during each fluence step the incident particles initiate a collision cascade in the target. At the end of each fluence step sputtering yield (chemical and physical), scattering coefficient, and implantation is calculated and then the sample is updated accordingly.

Depending upon the incident particle and target combination it is checked after each collision whether some thermal chemical reactions are possible or not. If yes, then the chemistry module is used to implement the reactions. Then the depth dependent out-diffusion probability of the reactions products is also calculated and this is used to calculate the thermal part of the erosion yield.

During the cascade the number of broken bonds is calculated for each layer. During the collision with the target atoms the incident particles lose their energy and at the end of the collision cascade they get implanted into the target. The number of the implanted hydrogen atoms are calculated for each layer. At the end of the fluence step the total number of implanted hydrogen atoms and bond breaking are used for the calculation of the kinetic part of the erosion yield.

The maximum amount of bonded hydrogen has an upper limit of 1/3. At the end of each fluence step the relative concentration of the bonded hydrogen is calculated and if it exceeds the upper limit the surplus hydrogen is treated as freely moving. This hydrogen can then diffuse through the target and leave the system. The corresponding interchange among the different carbon hybridization states is also done simultaneously. The surface binding energy (SBE) for the pure carbon target (mainly  $sp^2$  centers) is 7.37 eV [1].

When this sample of pur carbon is bombarded then  $sp^2$  as well as  $sp^3$  carbon centers are present and both of them should have the same SBE of 7.37 eV. In case of a-H:C sample the SBE of  $sp^3$  carbon centers changes due to the presence of hydrogen. At higher concentration of hydrogen the SBE of  $sp^3_H$  remains 5.00 eV where as for  $sp^3$  it depends on the ratio of  $sp^3_H : (sp^3 + sp^3_H)$ . For example if one start with a pure carbon target, as the system evolves the relative concentrations of  $sp^2$ ,  $sp^3$  and  $sp^3_H$  changes and accordingly the SBE of  $sp^3$  also varies.

Finally all the counters for the bond breaking and hydrogen implantation in each layer are reset to zero.

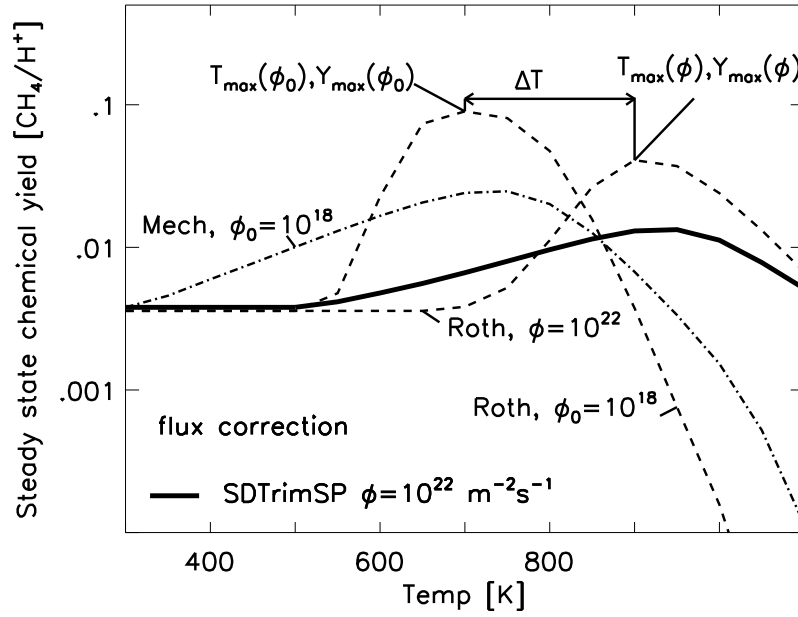


Figure 18: Correction of thermal erosion yield of Mech [31] at a H flux  $\Phi = 10^{18} m^{-2} s^{-1}$  to get values at  $\Phi = 10^{22} m^{-2} s^{-1}$  (SDTrimSP) using the analytical formula by Roth [29].



Fig.19 shows a comparison of calculated results of D on C target with measurements at two different temperatures as a function of the energy. Although the calculated results at room temperature are at the lower limit, the agreement is very good.

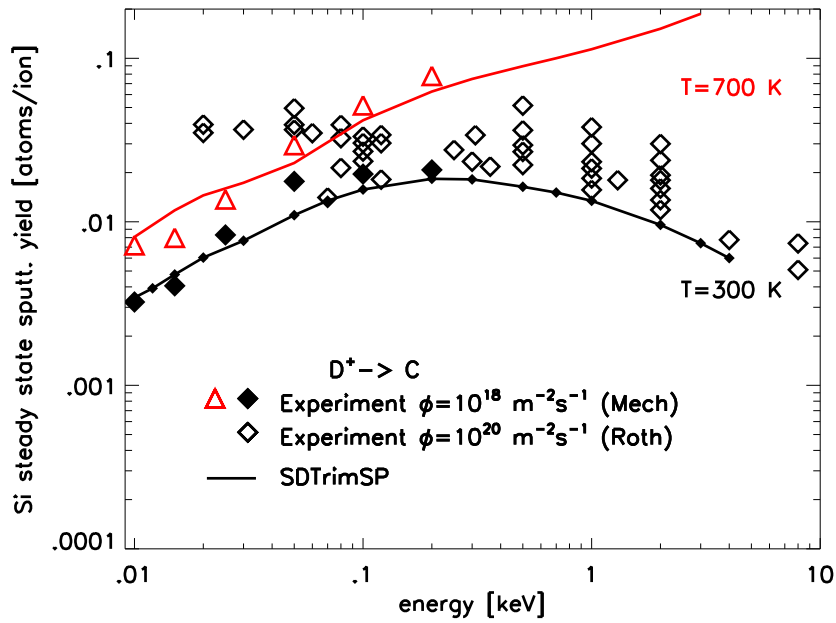


Figure 19: Calculated steady state sputtering yields of D versus the incident energy of D on a C target at normal incidence compared with experimental data [29].

## 8. Sensitivity studies for D on Be and D on W

### 8.1. Number of incident particles

In a Monte Carlo code the number of test particles defines the accuracy of the results. Fig. 20 shows the value of the sputtering yield for D on Be at normal incidence for four different energies as a function of the number of incident D particles. Fig. 21 - 22 show the relative and absolute error of the yields for this example. In this particular case the number of incident projectiles should be more than  $10^7$  particles to obtain sufficiently good statistic estimates.

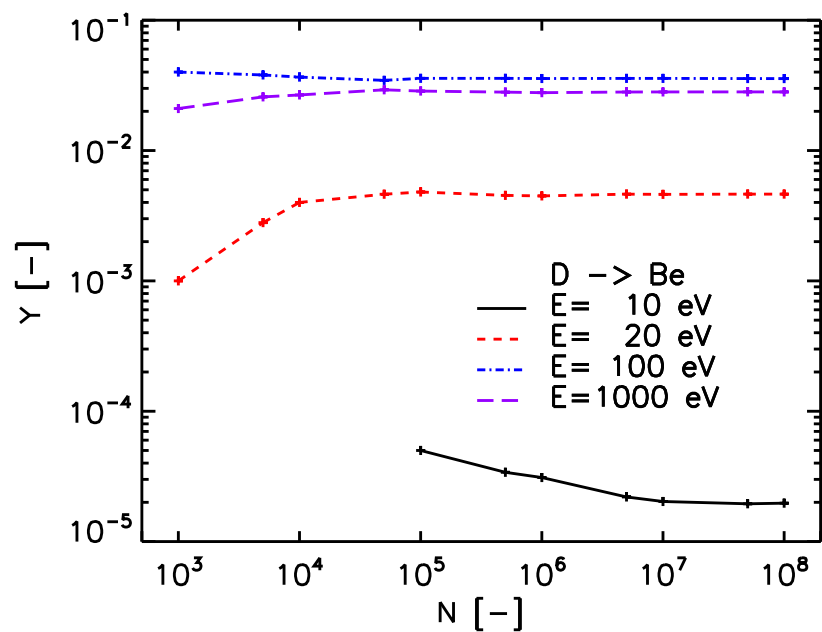


Figure 20: Calculated absolute Yield depending on number of incident particles of D on a Be target at normal incidence for four different energies.

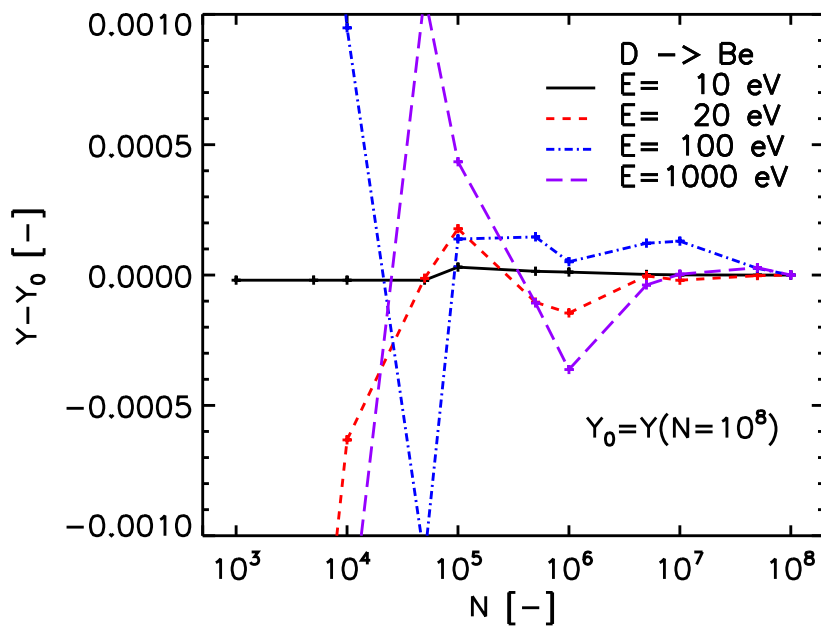


Figure 21: Absolute difference of  $Y$  to  $Y_0$  as a function of the number of incident  $D$  particles on a  $Be$  target at normal incidence for four different energies

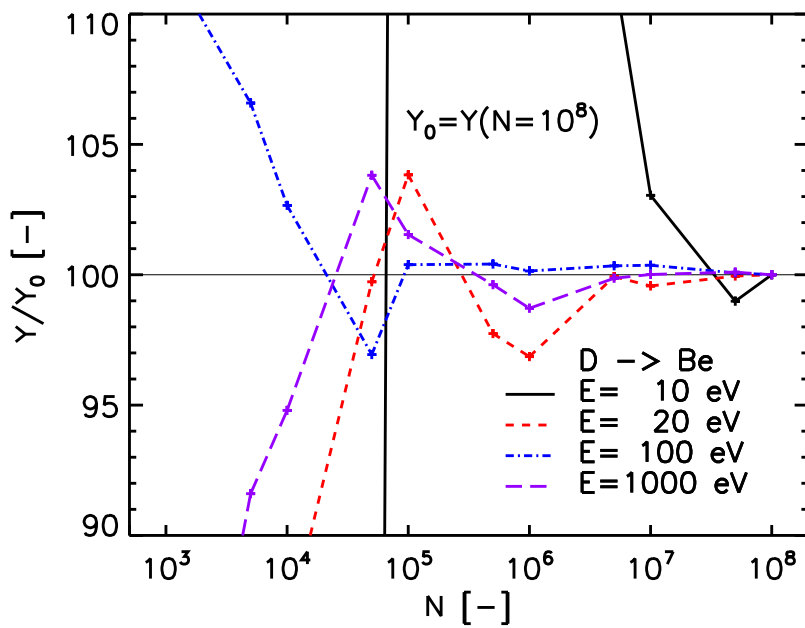


Figure 22: Relative deviation  $Y$  to  $Y_0$  as a function of the number of incident  $D$  particles on a  $Be$  target at normal incidence for four different energies

## 8.2. Surface binding energy

The user can choose from three methods to calculate the surface binding energy (*sbe*) of atoms in a target.  $Es$  is the atomic surface binding energy for each species and  $q$  the atomic fraction. For a stationary case  $q_D = 0$ ,  $q_{Be} = 1$  and  $q_W = 1$ .

$$\begin{aligned} Es_D &= 0.10 \text{ eV} \\ Es_{Be} &= 3.31 \text{ eV} \\ Es_W &= 8.79 \text{ eV} \end{aligned} \tag{8.21}$$

**model1:**

$$\begin{aligned} sbe_D &= Es_D = 0.10 \text{ eV} \\ sbe_{Be} &= Es_{Be} = 3.31 \text{ eV} \\ sbe_W &= Es_W = 8.79 \text{ eV} \end{aligned} \tag{8.22}$$

**model2 for D on Be:**

$$\begin{aligned} sbe_D &= q_D \cdot Es_D + q_{Be} \cdot Es_{Be} = 3.31 \text{ eV} \\ sbe_{Be} &= q_D \cdot Es_D + q_{Be} \cdot Es_{Be} = 3.31 \text{ eV} \end{aligned} \tag{8.23}$$

**model2 for D on W:**

$$\begin{aligned} sbe_D &= q_D \cdot Es_D + q_W \cdot Es_W = 8.79 \text{ eV} \\ sbe_W &= q_D \cdot Es_D + q_W \cdot Es_W = 8.79 \text{ eV} \end{aligned} \tag{8.24}$$

**model3 for D on Be:**

$$\begin{aligned} sbe_D &= q_D \cdot Es_D + q_{Be} \cdot 0.5(Es_D + Es_{Be}) = 1.705 \text{ eV} \\ sbe_{Be} &= q_D \cdot 0.5(Es_D + Es_{Be}) + q_{Be} \cdot Es_{Be} = 3.31 \text{ eV} \end{aligned} \tag{8.25}$$

**model3 for D on W:**

$$\begin{aligned} sbe_D &= q_D \cdot Es_D + q_W \cdot 0.5(Es_D + Es_W) = 4.445 \text{ eV} \\ sbe_W &= q_D \cdot 0.5(Es_D + Es_W) + q_W \cdot Es_W = 8.79 \text{ eV} \end{aligned} \tag{8.26}$$

The surface binding energies *sbe* of Be and W are their atomic surface binding energies, which are unaffected by the choice of the model. Only the D binding energy is changed and therefore only the scattering coefficient  $R$  changes, see Fig. 23 - 26. All calculations used the ' $Kr - C$ ' potential, surface-binding-model 3 and the integration-method 'MAGIC'.

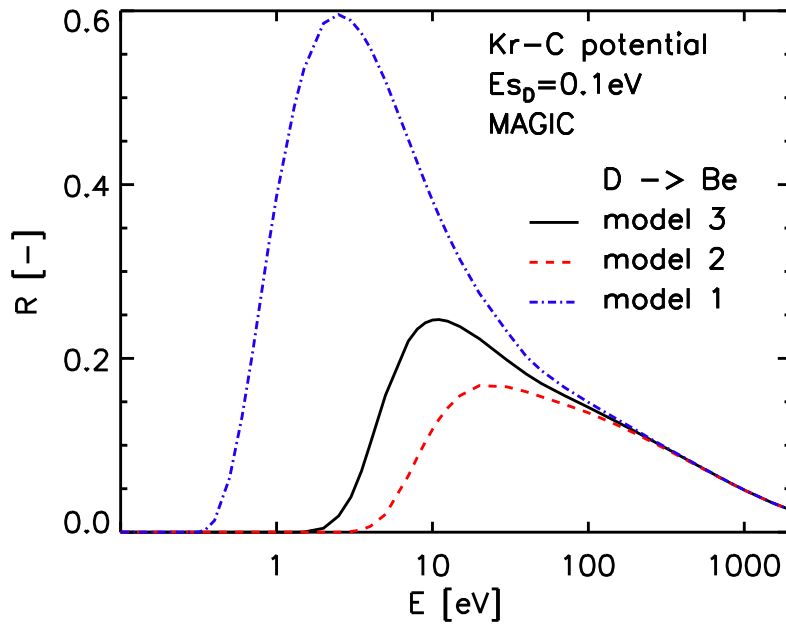


Figure 23: Calculated reflection coefficient  $R$  depending on surface binding model of D on a Be target at normal incidence.

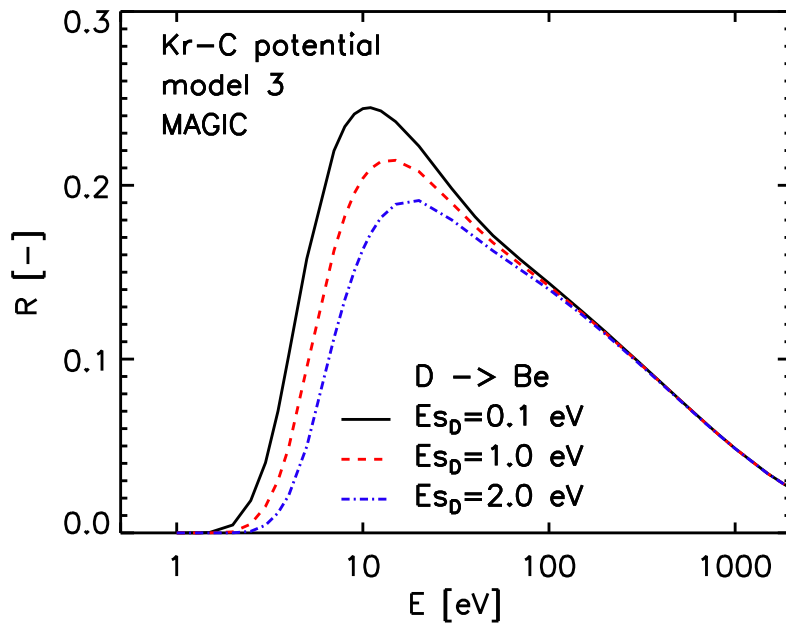


Figure 24: Calculated reflection coefficient  $R$  for three different surface binding energies of D

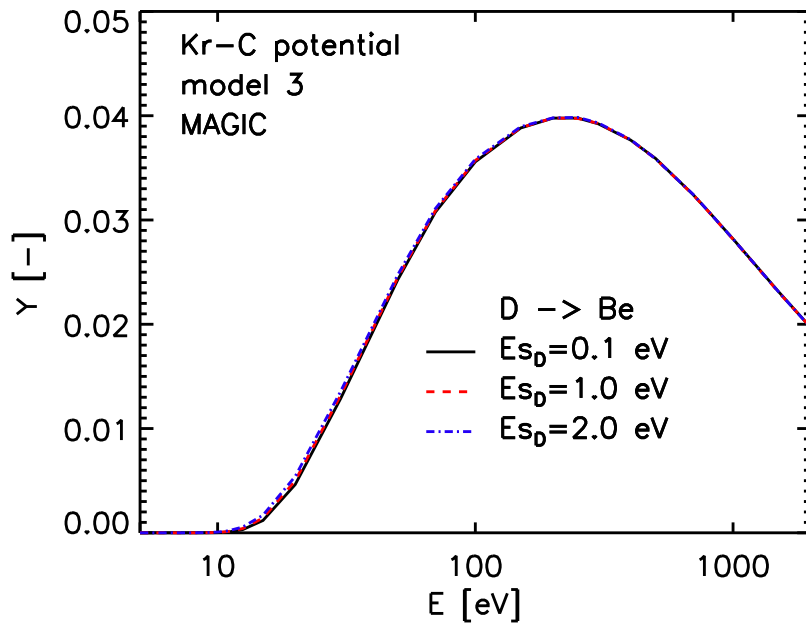


Figure 25: Calculated sputtering yield  $Y$  for three different surface binding energy of D

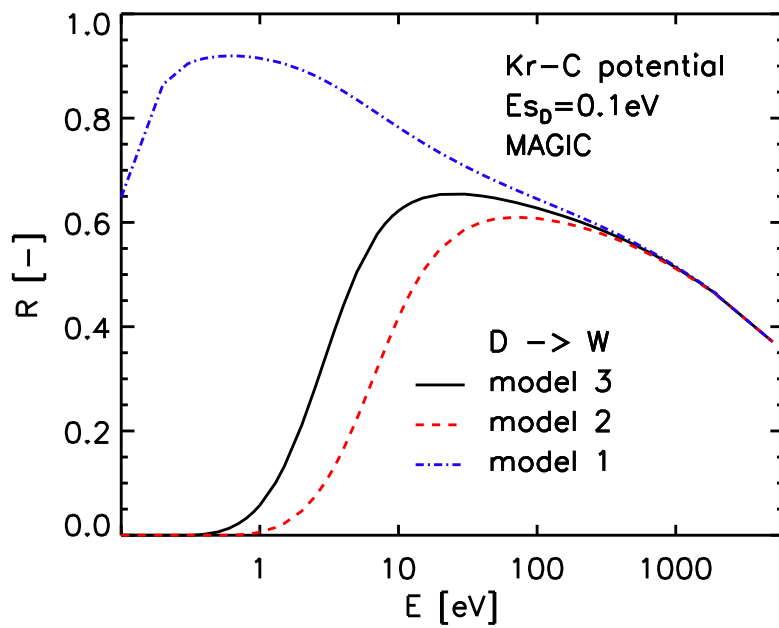


Figure 26: Calculated reflection coefficient  $R$  depending on surface binding model of D on a W target at normal incidence

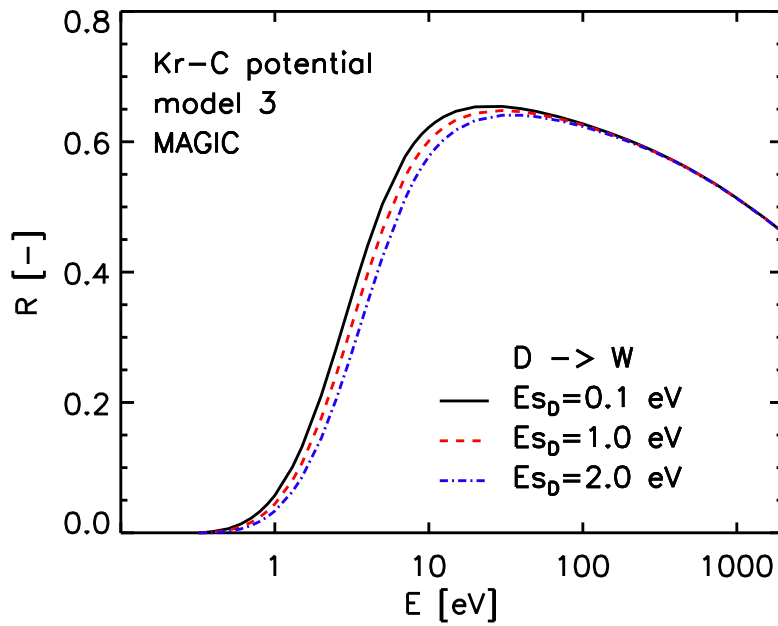


Figure 27: Calculated reflection coefficient  $R$  for three different surface binding energies of D

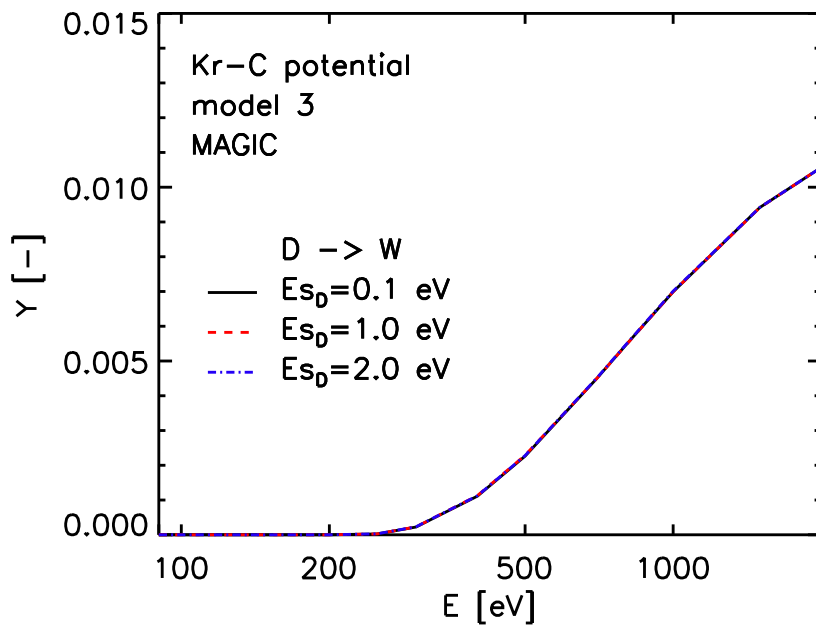


Figure 28: Calculated sputtering yield  $Y$  for three different surface binding energy of D

### 8.3. Integration methods

The scattering angle  $\vartheta$  in the center-of-mass system is determined by [1]

$$\vartheta = \pi - 2p \int_R^{\infty} r^{-2} g(r)^{-1} dr \quad (8.27)$$

$$g(r) = \sqrt{1 - \frac{p^2}{r^2} - \frac{V(r)}{E_r}}, \quad g(R) = 0 \quad (8.28)$$

where  $p$  is the impact parameter,  $R$  is the distance of closest approach of the two collision partners,  $V(r)$  is the interaction potential and  $E_r$  is the energy in the center-of-mass system.

The other important integral is the time-integral  $\tau$

$$\tau = \sqrt{r^2 - p^2} - \int_R^{\infty} g(r)^{-1} - f(r)^{-1} dr \quad (8.29)$$

$$f(r) = \sqrt{1 - \frac{p^2}{r^2}} \quad (8.30)$$

The numerical solution of the integrals is possible with the Gauss-Mehler quadratur [14], the Gauss-Legendre quadratur [1] or the 'magic' algorithm from Biersack [1]. The results of the different integration methods are shown in Figs. 29 - 30.

All calculation were made with the ' $Kr - C$ ' Potential and surface-binding-model three. The surface-binding-energy of deuterium was 0.1 eV. The difference between the integration methods of Gauss-Mehler and Gauss-Legendre is small. The method 'MAGIC' is only only a approximate method and it agrees well only in some energy ranges.



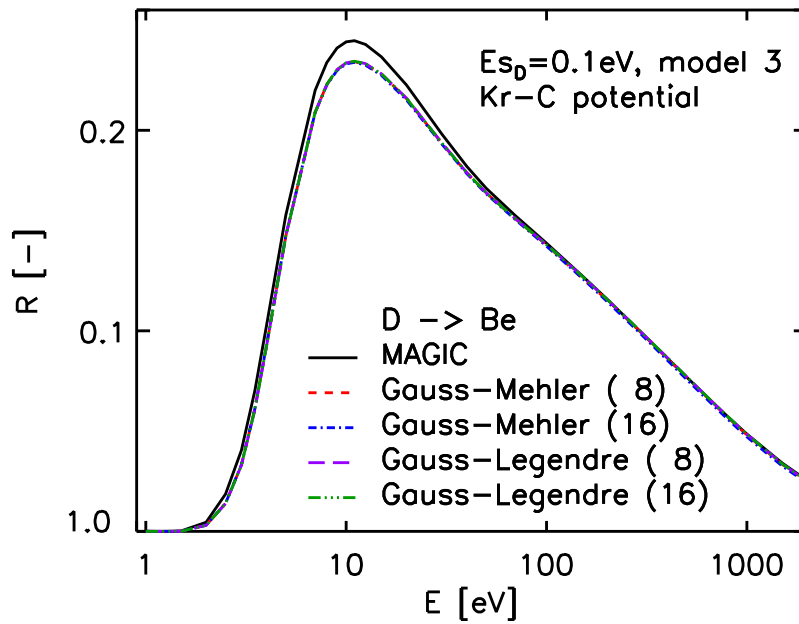


Figure 29: Calculated reflection coefficient  $R$  D on Be for three different integration methods. Gauss-Mehler and Gauss-Legendre were calculated with 8 and 16 numbers of steps.

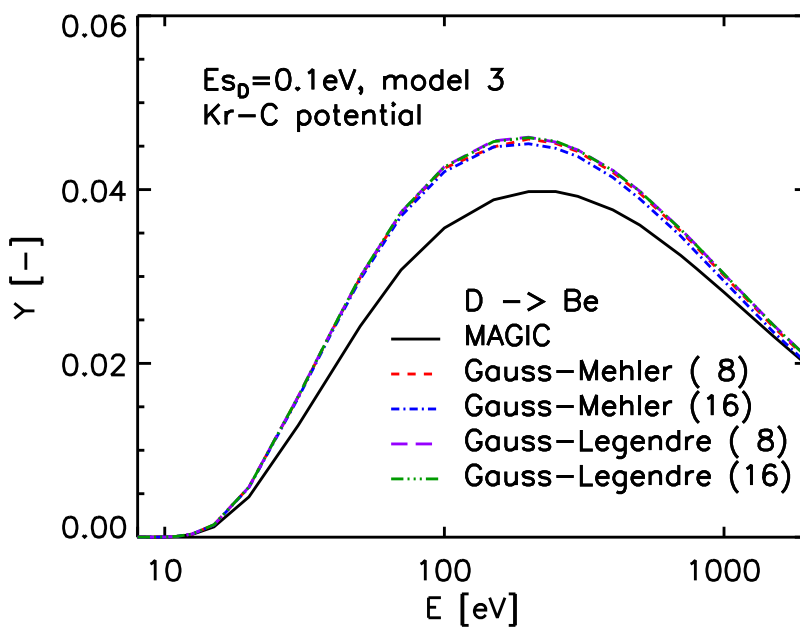


Figure 30: Calculated sputtering yield  $Y$  D on Be for three different integration methods. Gauss-Mehler and Gauss-Legendre were calculated with 8 and 16 numbers of steps.

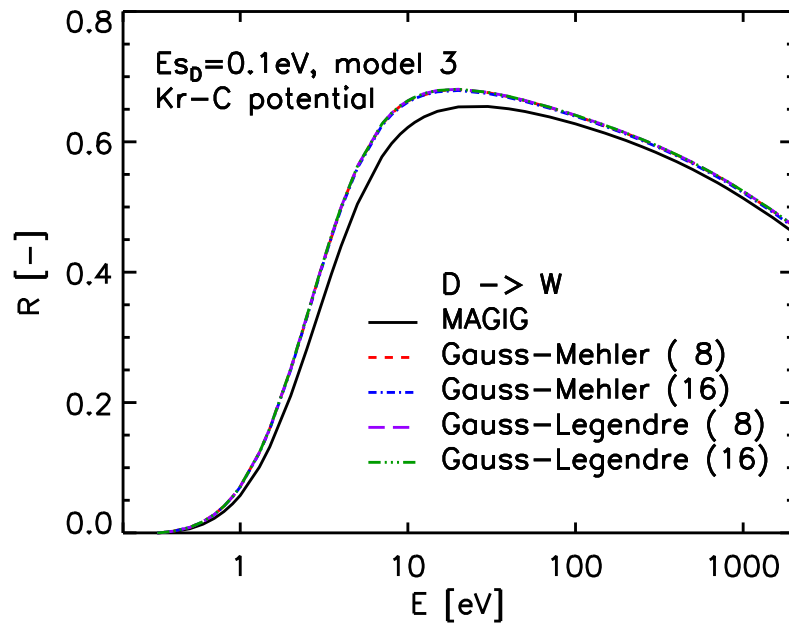


Figure 31: Calculated reflection coefficient  $R$  D on W for three different integration methods. Gauss-Mehler and Gauss-Legendre were calculated with 8 and 16 numbers of step.

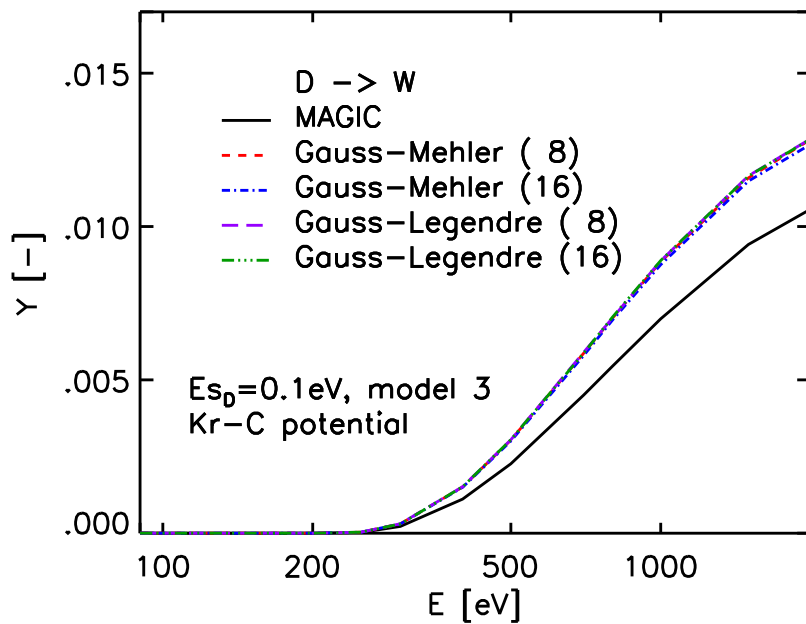


Figure 32: Calculated sputtering yield  $Y$  D on W for three different integration methods. Gauss-Mehler and Gauss-Legendre were calculated with 8 and 16 numbers of step.

## 8.4. Sreened coulomb potentials

The sreened coulomb potentials  $V(r)$ , see [1], can be written in the form

$$V(r) = \frac{Z_1 \cdot Z_2 \cdot e^2}{r} \cdot \Phi\left(\frac{r}{a}\right) \quad (8.31)$$

with  $Z_1$  charge of projectile,  $Z_2$  charge of target atom and  $a$  the screening length.

$$e^2 = 14.399651 \text{ eV } \text{Å} \quad (8.32)$$

for the **Krypton-carbon** potential:

$$\Phi\left(\frac{r}{a}\right) = 0.191e^{-0.278r/a} \cdot .474e^{-0.637r/a} \cdot .335e^{-1.919r/a} \quad (8.33)$$

for the **Moliere** potential:

$$\Phi\left(\frac{r}{a}\right) = .35e^{-.279r/a} \cdot .55e^{-0.3r/a} \cdot .10e^{-1.2r/a} \cdot 0.191e^{-6.0r/a} \quad (8.34)$$

for the **ZBL** potential:

$$\Phi\left(\frac{r}{a}\right) = .02817e^{-0.2016r/a} \cdot .2802e^{-0.4029r/a} \cdot .5099e^{-0.9423r/a} \cdot .1818e^{-3.2r/a} \quad (8.35)$$

for the **Nakagava-Yamamura** potential:

$$\Phi\left(\frac{r}{a}\right) = e^{(-A \cdot (r/a) + B \cdot (r/a)^{1.5} - C \cdot (r/a)^2)} \quad (8.36)$$

$$A = 1.51$$

$$B = 0.763 * (Z_1^{0.169} + Z_2^{0.169}) / (Z_1^{0.307} + Z_2^{0.307}) \quad (8.37)$$

$$C = 0.191 * ((Z_1^{0.0481} + Z_2^{0.0481}) / (Z_2^{0.307} + Z_2^{0.307}))^{4./3}.$$

All calculations were done with Gauss-Legendre integration and surface-binding-model three. The surface-binding-energy of deuterium was 0.1 eV. The difference between the different potentials is relative small.

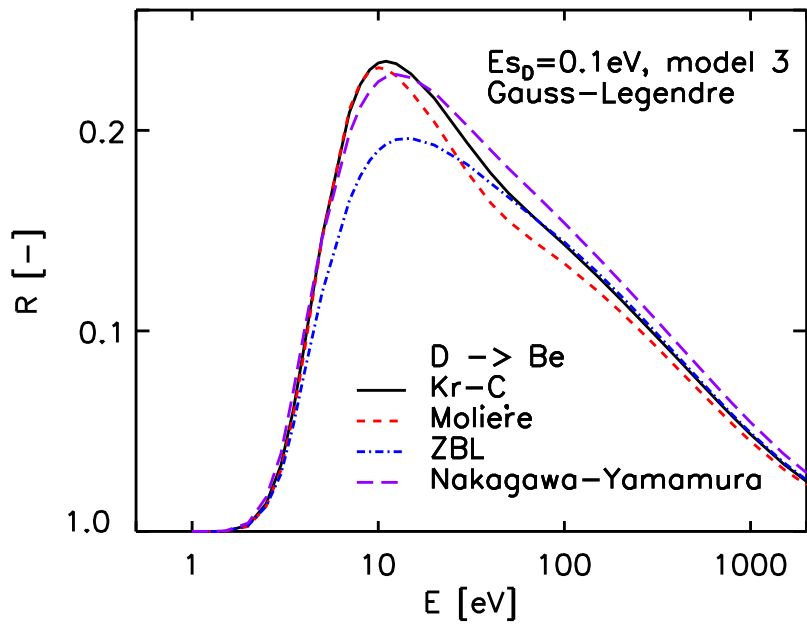


Figure 33: Calculated reflection coefficient  $R$  of D on Be for four different potentials.

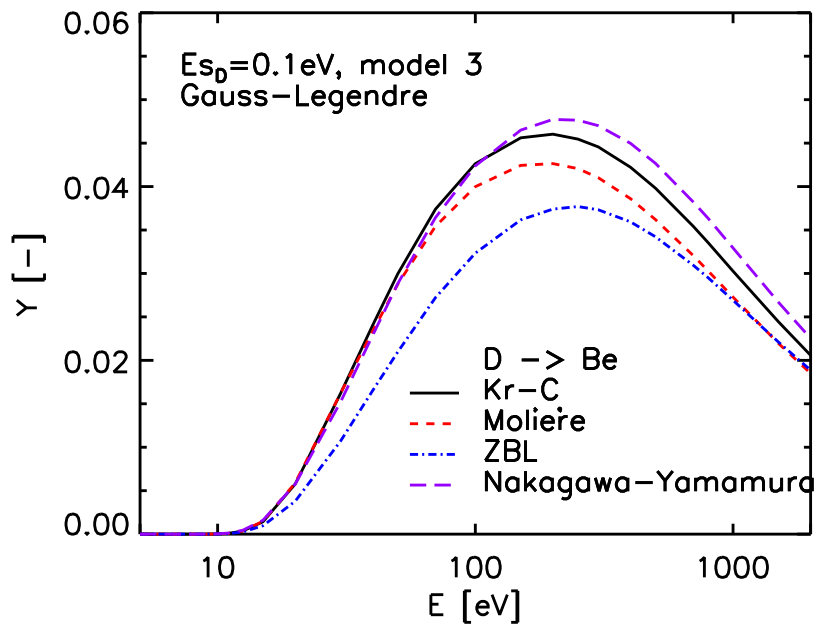


Figure 34: Calculated sputtering yield  $Y$  of D on Be for four different potentials.

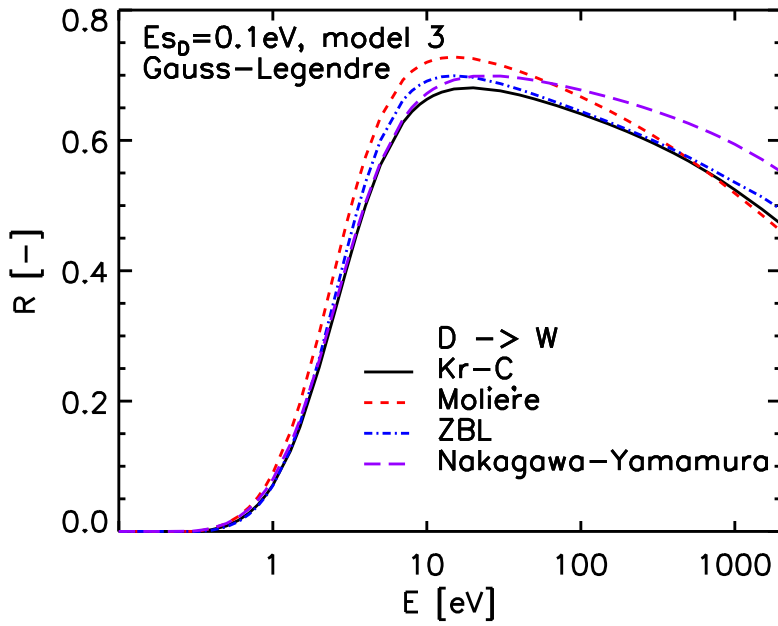


Figure 35: Calculated reflection coefficient  $R$  of D on W for four different potentials.

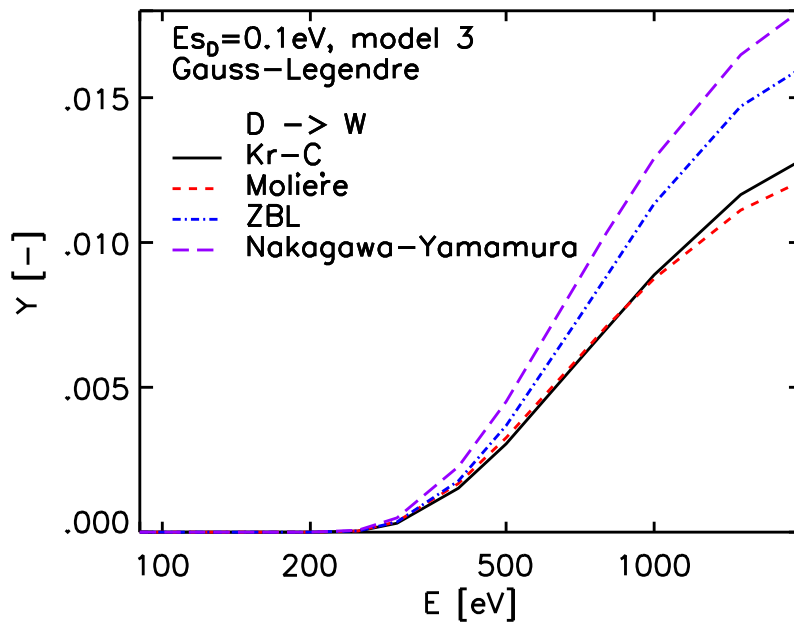


Figure 36: Calculated sputtering yield  $Y$  of D on W for four different potentials.

## 9. New input variables in 'tri.inp'

The new optional input parameters compared with version 4.15, [27] are listed in Tab. 4. In the appendix Tab. 8 - Tab. 15 discuss the new parameters.

variable	default value	description
lmatout_log_energ	.false.	energy spacing = .false. : linear energy intervals = .true. : logarithmic energy intervals
lmatout_cos_angle	.false.	angular spacing = .false. : angle in degree intervals = .true. : cosine intervals
lenergy_distr	.false.	output of energy distribution in target in E.distr_stop.dat of projectiles and recoils atoms using the chosen energy spacing (stop, electric loss and elastic nuclear loss energies)
loutgas	.false.	calculation with out-gasing transport and diffusion
diff_koeff1(ncp)	1.0	transport-coefficient if loutgas true [ $\text{\AA}^3/\text{ion}$ ]
diff_koeff2(ncp)	1.0	diffusion-coefficient if loutgas true [ $\text{\AA}^4/\text{ion}$ ]
qu_int	.false.	linear interpolation of atomic fraction (qu) inside of interval
lchem_ch	.false.	calculation with chemical erosion H on C(SP2,SP3,SP3H), D on C(SP2,SP3,SP3H)
flux	1.0	flux of incident atoms
k_start	0	start counter intern
text		comment in NAMELIST
case_e0	0	flag for the choice of the incident energy = 6 : distribution of alpha and energy, input-file: 'ene_ang.inp'
case_e0	0	flag for the choice of the incident energy = 6 : distribution of alpha and energy, input-file: 'ene_ang.inp'
case_alpha	0	flag for the choice of the angle of incidence = 6 : distribution of alpha and energy, input-file: 'ene_ang.inp'

Table 4: New optional input variables with default values

## References

- [1] W. Eckstein, Computer Simulation of Ion-Solid Interactions, Springer Series in Material Science, Vol. 10, Springer Berlin, Heidelberg 1991
- [2] J. P. Biersack, W. Eckstein, Appl. Phys. A 34 (1984) 73
- [3] W. Möller, W. Eckstein, Nucl. Instrum. Meth. B 2 (1984) 814
- [4] W. Möller, W. Eckstein, J. P. Biersack, Comput. Phys. Comm. 51 (1988) 355
- [5] H. H. Andersen, J. F. Ziegler: In Hydrogen Stopping Powers and Ranges in All Elements, The Stopping and Range of Ions in Matter, Vol.3, ed. by J. F. Ziegler (Pergamon, NewYork, 1977)
- [6] J. F. Ziegler: In Helium Stopping Powers and Ranges in All Elements, The Stopping and Range of Ions in Matter, Vol.4, ed. by J. F. Ziegler (Pergamon, NewYork, 1977)
- [7] W. D. Wilson, L. G. Haggmark, J. P. Biersack, Phys. Rev. 15 (1977) 2458
- [8] J. F. Ziegler, J. P. Biersack, U. Littmark: The Stopping and Range of Ions in Solids, The Stopping and Range of Ions in Matter, Vol.1, ed. by J. F. Ziegler (Pergamon, NewYork, 1985)
- [9] G. Molière, Z. Naturforsch. A2 (1947) 133
- [10] W. Eckstein, S. Hackel, D. Heinemann, B. Fricke, Z. Phys. D 24 (1992) 171
- [11] J. P. Biersack, L. G. Haggmark, Nucl. Instrum. Meth. 174 (1980) 257
- [12] K. Mehler, J. Reine Angew. Math. 63 (1864) 152
- [13] Z. Kopal, *Numerical Analysis*, Chapman and Hall, London 1961, p. 367 ff.
- [14] H. G. Schlager, W. Eckstein, IPP-Report 9/69, Garching 1991
- [15] M. T. Robinson: Tables of Classical Scattering Integrals, Oak Ridge Natl. Lab., Oak Ridge, Tennessee (1970)
- [16] R. Vichev, W. Eckstein, Nucl. Instrum. Meth. B 102 (1995) 272
- [17] R. Vichev, W. Eckstein, Nucl. Instrum. Meth. B 122 (1997) 215
- [18] W. Eckstein, R. Dohmen, Nucl. Instrum. Meth. B 129 (1997) 327
- [19] R. Becerra-Acevedo, J. Bohdansky, W. Eckstein and J. Roth, Nucl. Instrum. Meth. B 2 (1984) 631
- [20] W. Eckstein, Nucl. Instrum. Meth. B 27 (1987) 78

- [21] S. T. Nakagawa, Y. Yamamura, *Radiat.Eff.*105, 239(1988)
- [22] S. T. Nakagawa, *Radiation Effects and Defects in Solids*, Vol.116 (1991), page 21-28
- [23] A. Mutzke, W. Eckstein, *Nucl. Instr. and Meth. B* 266(2008) 872
- [24] K. Wittmaack, *Nucl. Instr. and Meth. B* 267(2009) 2846-2857
- [25] N. Menzel and K. Wittmaack, *Nucl. Instr. and Meth. in Phys. Res. B*7/8 (1985) 366-370
- [26] P. Blank, K. Wittmaack and F. Schulz *Nucl. Instr. and Meth.* 132 (1976) 387-392
- [27] W. Eckstein, R. Dohmen, A. Mutzke, R. Schneider, Report IPP 12/3, Garching, (2007)
- [28] W. Möller, W. Eckstein, Report IPP 9/64, Garching, (1988)
- [29] J. Roth, C. Garcia-Rosales ,*Nuclear Fusion* 36 (1996) 1647
- [30] C. Hopf, A. von Keudell, W. Jacob, *J.Appl.Phys.* 94 (2003) 2373-2380
- [31] B. V. Mech, A. A. Haasz and J. W. Davis , *J. Appl. Phys.* 84 (1998) 1655-1669
- [32] A. Rai, A. Mutzke and R. Schneider, *Nucl. Instr. Meth. B* 268 (2010) 2639-2648



## A. Global parameters

parameter	value	description	program
ncpm	8	maximum number of elements	param.F90
nqxm	2000	maximum number of depth intervals	param.F90
pemax	32	maximum number of PEs	work.F90
ntpmax	16384	size of global task queue	task_descr.F90
ntqmax	131072	size of local task queue	task_descr.F90
nhmax	8192	maximum number of trace records to be recorded	task_descr.F90

Table 5: Global parameters (set in programs)

## B. Input variables in 'tri.inp'

### B.1. Necessary input variables

The sequence of the input values in the input file is arbitrary (namelist)

variable	description
alpha0(ncp)	angle of incidence (degree) of ncp species in case_alpha=0,5
e0(ncp)	energies (eV) of projectiles (qubeam > 0.) for case_e0=0,5 $e0 = ttemp * boltzm$ ( $e0 < 0$ ) of projectiles for case_e0=2,3
flc	temperature (eV) (kT) ( $e0 > 0$ ) of projectiles for case_e0=2,3
ipot	incident fluence ( $10^{16} atoms/cm^2$ or $atoms/A^2$ ) interaction potential: = 1 : KrC = 2 : Moliere = 3 : ZBL = 4 : Nakagawa-Yamamura = 5 : Si-Si = 6 : power

Table 6: Necessary input variables (no default values)

variable	description
isbv	surface binding model, determines the composition dependent surface binding energy $sbv(ncp,ncp)$ from the elemental surface binding energies $e\_surfb(ncp)$ taken from table1 = 1 : $sbv(ip,jp)=e\_surfb(jp)$ for $ip=jp$ , =0 else = 2 : $sbv(ip,jp)=e\_surfb(jp)$ for all $ip, jp$ = 3 : $sbv(ip,jp)=0.$ , if $e\_surfb(ip)=0$ or $e\_surfb(jp)=0$ $sbv(ip,jp)=0.5*(e\_surfb(ip)+e\_surfb(jp))$ else = 4 : $sbv(ip,jp)=f(e\_surfb,qu,delta hf)$ for solid/solid compound = 5 : $sbv(ip,jp)=f(e\_surfb,qu,delta hf,delta hd)$ solid/gas compound
ncp	number of species (projectiles + target species) more than one projectile species is allowed
nh	number of histories (projectiles)
nqx	number of depth intervals of the target (discretization)
qubeam(ncp)	projectile atomic fractions (in incident beam) of ncp species, $qubeam > 0.$ , Note: $\sum(qubeam(1:ncp))=1$ $qubeam \leq 1.$ for projectiles $qubeam = 0.$ for target atoms
qu(ncp)	initial target atomic fractions of ncp species in case of homogeneous initial composition ( $iq0 = 0$ )
symbol(ncp)	ncp chemical symbols of elements according to table1 (special symbol: 'H','D','T','He3','He','P_w','P_r', carbon with different density: 'C_a','C_g','C_f','C_d', hybridization state of carbon Sp2,Sp3,Sp3H)
two_comp	symbol of two-component target according to table.compound (e.g. $two\_comp = 'Ta2O5'$ ) Note: only selected compounds in table.compound

Table 7: Necessary input variables (no default values) (continue)

## B.2. Optional input variables

These values have default values (see default\_init.txt). If values different from the default values are needed, then these values have to be given explicitly in the input file.

variable	default value	description
angleinp	'./'	directory of inputfile 'angle.inp' (see also: layerinp, tableinp, energyinp)
a_mass(ncp)	table	mass (in amu) of ncp elements; default from table1
a_num_z(ncp)	table	atomic number of ncp elements; default from table1
case_alpha	0	<p>flag for the choice of the angle of incidence</p> <p>= 0 : angle of incidence (degree) counted from the surface normal (azimuthal angle <math>\phi = 0</math>)  <math>\alpha_0 = 0 \dots 90</math> (starting above surface)  <math>\alpha_0 = 90 \dots 180</math> (starting in solid)</p> <p>= 1 : random distribution of angles of incidence (only from above surface) (<math>\alpha</math> and <math>\phi</math> random)</p> <p>= 2 : cosine distribution of angles of incidence (only from above surface)</p> <p>= 3 : cosine distribution of angles of incidence  <math>\alpha = 0 \dots \pi/2</math>, max: by 0 <math>\phi = 0 \dots 2\pi</math></p> <p>= 4 : input of a given incident angular distribution from file angle.inp</p> <p>= 5 : series of calculations with different angles of incidence            ( <math>\alpha = (i - 1) \cdot \alpha_0</math>; <math>i = 1, \text{ number\_calc}</math> )            output : output.* dat            default set :lmatrices = .false.                      ltraj_p = .false., ltraj_r = .false.                      lparticle_r = .false., lparticle_p = .false.                      case_e0 = 0            (note: all *.dat outputfile from last calculation)</p> <p>= 6 : distribution of <math>\alpha</math> and energy            input-file: 'ene_ang.inp'</p>

Table 8: Optional input variables with default values

variable	default value	description
case_e0	0	<p>flag for the choice of the incident energy</p> <p>= 0 : fixed incident energies(eV) of projectiles (qubeam&gt;0)</p> <p>= 1 : input of a given energy distribution from file energy.inp</p> <p>= 2 : temperature (eV) of a Maxwellian velocity distribution of projectiles</p> <p>= 3 : temperature (eV) of a Maxwellian energy distribution of projectiles</p> <p>= 5 : series of calculations with different projectile energies</p> <p>e0(1)&gt;0: linear energy= <math>i \cdot e0</math> ; <math>i = 1, \text{ number\_calc}</math></p> <p>e0(1)&lt;0: logarithmic energy= <math>10^{(i-1)} \cdot e0</math>; <math>i = 1, \text{ number\_calc}</math></p> <p>output: output.*dat</p> <p>default set: lmatrices = .false. ltraj_p = .false., ltraj_r = .false., lparticle_r = .false., lparticle_p = .false., case_alpha = 0 (note: all *.dat file from last calculation)</p> <p>= 6 : distribution of alpha and energy, input-file: 'ene_ang.inp'</p>
case_layer_thick	0	<p>mixing chema of target</p> <p>0 mixing lauer with neighbour lauer, if thick: 150% or 50%</p> <p>1 mixing to constant layer thick , if one layer thick: 110% or 90%</p>
ca_scre(ncp,ncp)	1.	<p>correction factor for the screening length in the interaction potential (not applicable for KrC and ZBL potentials)</p>
charge(ncp)	0	<p>charge of species if case_e0=2,3 and sheath&gt;0 (plasma)</p> <p><math>\geq 1</math>. for qubeam&gt;0 (projectiles)</p> <p>= 0. for qubeam=0 (target atoms)</p>

Table 9: Optional input variables with default values (continue)

variable	default value	description
ck_elec(ncp,ncp)	1.	correction factor for the inelastic energy loss; correction factors for hydrogen (below 25 keV) are given in table3
deltahd(ncp)		heat of dissociation (eV) of a molecular target default from table1
deltahf		heat of formation (eV) of a molecular target default from table1
diff_koeff1(ncp)	1.0	transport-coefficient if loutgas true [ $A^3/ion$ ] (see also: loutgas)
diff_koeff2(ncp)	1.0	diffusion-coefficient if loutgas true [ $A^4/ion$ ] (see also: loutgas)
dist_nx	60	x-size of the matrix of energy distribution in target
dist_ny	60	y-size of the matrix of energy distribution in target
dist_nz	60	z-size of the matrix of energy distribution in target
dist_delta	2.0	distance between the matrix points of energy distribution in target
dns0(ncp)		atomic density ( $atoms/A^3$ ) of ncp elements; default from table1
dsf	5.	average depth (A) for surface composition
e_bulkb(ncp)	0.	bulk binding energy; if e_bulkb>0., e_bulk has to be subtracted from the surface binding energy e_surfb
e_cutoff(ncp)		cutoff energy (eV) of ncp species; defaults from table1 (0.05 eV for noble gases; 1 eV for H, D, T; e_surf - 0.05 eV for selfbombardment)
e_displ(ncp)		displacement energy (eV); default from table1 (if in table1 e_displ=0 then e_displ=15)
e_surfb(ncp)		surface binding energy (eV) (heat of sublimation); default from table1
energyinp	'./'	directory of inputfile 'energy.inp' (see also: layerinp, tableinp, angleinp)
flux	1.0	flux of incident atoms ( $atoms/A^2/s = 10^{20}atoms/m^2/s$ )
idrel	1	mode of simulation = 0 : full dynamic calculation (TRIDYN) > 0 : suppression of dynamic relaxation (TRIM), full static calculation < 0 : suppression of dynamic relaxation and cascades static calculation (TRIM) only projectiles (no recoils) are followed

Table 10: Optional input variables with default values (continue)

variable	default value	description
idout	-1	control output, determines the outputfiles: E0_31_target.dat, E0_34_moments.dat, partic*.dat, trajec*.dat and restart_file = -1 : output after each fluence step of nh/100, 100 fluence steps = 0 : output only after the last fluence step > 0 : output after each idout'th fluence step and last step
iintegral	0	integration method = 0 : MAGIC, only valid for KrC, ZBL, Moliere = 1 : Gauss-Mehler quadrature, ipivot $\geq$ 8 recommended = 2 : Gauss-Legendre quadrature, ipivot $\leq$ 16
imcp	0	flag indicating whether (fib)-moments of distributions are calculated = 0 : no moment calculation = 1 : moments of depth distributions for all projectiles (qubeam>0.)
inel0(ncp)	3	inelastic loss model = 1 : Lindhard-Scharff; nessary condition: $E < 25 \cdot Z^{4/3} \cdot M$ (in keV) where E, Z, M are the energy, the atomic number and the atomic mass of the moving particle = 2 : Oen-Robinson; nessary condition: $E < 25 \cdot Z^{4/3} \cdot M$ (in keV) = 3 : equipartition of 1 and 2 = 4 : high energy hydrogen (H,D,T) (energy > 25 keV) values from table3 = 5 : high energy helium (He3,He) (energy > 100 keV) values from table4

Table 11: Optional input variables with default values (continue)

variable	default value	description
ioutput_hist(6)	10	number of traced trajectories for: stopped, backscattered and transmitted projectiles, stopped, backscattered, transmission sputtered recoils (see also: lttraj_p, lttraj_r)
ioutput_part(6)	10	number of traced particles for: stopped, backscattered and transmitted projectiles, stopped, backscattered, transmission sputtered recoils (see also: lparticle_p, lparticle_r)
ipivot	16	number of pivots in the Gauss-Mehler and Gauss-Legendre integration, the minimum number is 4 (larger numbers in- crease the computing time)
iq0	0	initial composition flag < 0 : initial depth dependent composition taken from file layer.inp = 0 : initial composition homogeneous, one layer with constant depth intervals
irand	1	random seed
irc0	-1	flag for subthreshold recoil atoms < 0 : subthreshold recoil atoms free $\geq 0$ : subthreshold atoms bound
isot(ncp)	0	flag for isotope mass = 0 : natural isotope mixture (mass from table1) = 1 : isotope masses and natural abundances from table2 (valid for projectiles as well as for target species)
i_two_comp	1	method to determine the densities dns0(:) from the compound density in a two-component target (ta- ble.compound) =1 : dns0 for the first target species is set equal to the elemental density; necessary if the second element is a gas (e.g. Ta2O5) =2 : dns0 for the second target species is set equal to the elemental density =3 : iterative determination of both dns0(:); recom- mended if the elemental densities are different

Table 12: Optional input variables with default values (continue)

variable	default value	description
iwc=2	2	number of ring cylinders for weak simultaneous collisions for projectiles; for high energies (MeV H or He) iwc can be reduced to 1 or 0 to reduce computing time
iwcr=2	2	number of ring cylinders for weak simultaneous collisions for recoils
k_start	0	start counter intern
layerinp	'./'	directory of inputfile 'layer.inp' (see also: tableinp, angleinp, energyinp)
lchem_ch	.false.	calculation with chemical erosion H on C(SP2,SP3,SP3H), D on C(SP2,SP3,SP3H)
lenergy_distr	.false.	output of energy distribution in target in E_distr_stop.dat (energy of stop, electric loss and elastic nuclear loss)
lmatrices	.false.	.true. : output of matrices, if idrel /= 0 .false. : no matrix output
lmatout_log_energy	.false.	energy spacing = .false. : linear energy intervals = .true. : logarithmic energy intervals
lmatout_cos_angle	.false.	angular spacing = .false. : angle in degree intervals = .true. : cosine intervals
lmoments	.true.	output of moments for energy distributions (linear and logarithmic) of projectiles and recoils and for range distributions (linear) of projectiles .true. : moments are written .false. : moments are not written
loutgas	.false.	calculation with outgasing transport and diffusion (see also: diff_koeff1, diff_koeff2)
lparticle_p	.false.	.true. : output of projectile information .false. : no output of projectile information (see also: ioutput_part)
lparticle_r	.false.	.true. : output of recoil information .false. : no output of recoil information (see also: ioutput_part)

Table 13: Optional input variables with default values (continue)



variable	default value	description
ltableread	.true.	.true. : read from table1, table2, table3, table4 or table.compound .false. : no table read, a_num_z, a_mass, dns0, e_surfb e_displ have to be given <i>table1</i> : chemical symbol (symbol), nuclear charge (a_num_z), atomic mass (a_mass), mass density, atomic density (dns0), surface binding energy (e_surfb), displacement en- ergy (e_displ), cutoff energy (e_cutoff) <i>table2</i> : chemical symbol, nuclear charge, isotope mass, atomic weight (in amu), natural abundance <i>table3</i> : inelastic stopping coefficients for hydrogen: symbol, nu- clear charge, inelastic stopping coefficients a1 to a12 (ch_h), ck <i>table4</i> : inelastic stopping coefficients for helium: symbol, nuclear charge, inelastic stopping coefficients a1 to a9 (ch_he) <i>table.compound</i> : symbol of two-component target and physical values
ltraj_p	.false.	.true. : output of projectile trajectories .false. : no output of projectile trajectories (see also: numb_hist, ioutput_hist)
ltraj_r	.false.	.true. : output of recoil trajectories .false. : no output of recoil trajectories (see also: numb_hist, ioutput_hist)
lrestart	.false.	.true. : output of restartfiles after each idout .false. : no restart-files

Table 14: Optional input variables with default values (continue)

variable	default value	description
matrix_e_min	0	minimum of lin. energy distribution in matrices
matrix_e_max	max(e0)	maximum of lin. energy distribution in matrices
nm	-1	=-1 : not a molecular target > 1 : number of atoms in a two-component molecule
nr_pproj	10	number of projectiles between two target updates (idrel = 0)
numb_hist	20	number of traced trajectories of projectiles and recoils
number_calc	1	number of calculations if a series of calculations is carried out (case_e0 = 5 or case_alpha = 5)
nx_mat	1000	intervall of depth origin nx_mat= 100 intervall depth origin: input target ' nx_mat=1000 intervall depth origin: 1 A ' nx_mat=1001 intervall depth origin: 0.5 A '
qu_int	.false.	linear interpolation of atomic fractions between the depth intervals
qumax(ncp)	1.	maximum atomic fractions in the target for ncp species, if idrel=0
rhom		atomic density of a two-component target; default from table.compound [ $g/cm^3$ ]
sfin	0.	= 0 : no inelastic energy loss outside the target surface ( $x = 0$ .) = 1 : inelastic energy loss outside the target surface ( $-su > x > 0$ .)
shth	0.	= 0 : no sheath potential > 0 : sheath potential (eV), usually = $3 \cdot  e0 $ , only if case_e0=2,3 (Maxwellian distribution, plasma)
tableinp	'./tables'	directory of inputfile for tables (see also: layerinp, angleinp, energyinp)
text		comment in NAMELIST
ttarget		total target thickness in Angstrom (A)
ttemp	300.	target temperature, only of interest at high temperatures, it reduces the surface binding energy according to a Maxwellian energy distribution
x0(ncp)	0.	starting position of projectile $\leq 0$ . : outside the surface at $x = xc = -su$ > 0 . : inside the solid

Table 15: Optional input variables with default values (continue)

### B.3. Output format of energy distribution in the target

The option *lenergy\_distr* enables the calculation of the distribution of the energy input in the target. The total input energy is divided into energy of a division of stopped atoms, inelastic energy loss and elastic energy loss.

option: `lenergy_distr = .true.`

parameter: `dist_nx`  
`dist_ny`  
`dist_nz`  
`dist_delta`

output: `E_distr_all.dat` (output of total input energy )  
`E_distr_inel.dat` (output of inelastic energy loss)  
`E_distr_nucl.dat` (output of elastic energy loss)  
`E_distr_stop.dat` (output of energy from implanted particle)

The default values are:

variable	number	interval [Å]	distant [Å]	description
<code>dist_nx</code>	60	2	0 to 120	depth
<code>dist_ny</code>	60	2	-61 to 59	width
<code>dist_nz</code>	60	2	-61 to 59	length

Table 16: Default values for the option *lenergy\_distr*

### B.4. Output format of the depth of origin and penetration depth

In the static mode the output of the depth of origin and penetration depth are possible.

option: `lmatrices = .true.`

optional option: `lmatout_log_energ=.true.`

output: `morigin_ex_bs.dat` ...depth of origin of backscattered atoms dependent on energy  
`morigin_ex_ts.dat` ...depth of origin of transmitted sputtered atoms dependent energy  
`mpe_ex_p.dat` ...maximum of penetration of backscattered atoms  
`mepb.dat` ...path-length of backscattered atoms dependent energy  
`mept.dat` ...path-length of backscattered atoms dependent energy

## B.5. Output format of energy- and angle-distribution of scattered and sputtered atoms

### B.5.1. Output-matrix-file

The option *lmatrices* initiates output of the energy and angular distributions into four files.

option:            *lmatrices* =.true.

optional option: *lmatout\_cos\_angle*=.true.

output:            *meagb\_p.dat*    ...output of backscattered particles  
                  *meagb\_s.dat*    ...output of all backspattered particles  
                  *meagt\_p.dat*    ...output of all transmitted scattered particles  
                  *meagt\_s.dat*    ...output of all transmitted sputtered particles

### B.5.2. Post-processing of output-matrix-file with *readmatrix4.F90*

The FORTRAN program *readmatrix4.F90* in the directory *post* splits the four matrices into individual matrices.

post program :            */post/readmatrix4.F90*

input files:            *meagb\_p.dat*  
                          *meagb\_s.dat*  
                          *meagt\_p.dat*  
                          *meagt\_s.dat*



## C. Inputfile 'layer.inp'

number depth interval	thick-ness	composition of target (2:ncp) qu_2
1	0.10000E+02	0.94061E+00
1	0.10000E+02	0.89911E+00
1	0.10000E+02	0.88149E+00
1	0.10000E+02	0.86192E+00
3	0.20000E+02	0.85698E+00
3	0.20000E+02	0.84040E+00
1	0.20000E+02	0.83929E+00
1	0.20000E+02	0.82595E+00
1	0.20000E+02	0.82483E+00
1	0.30000E+02	0.81702E+00
1	0.30000E+02	0.81551E+00
1	0.30000E+02	0.81049E+00
100	0.30000E+02	0.80643E+00
0	0	0

Table 17: Inputfile 'layer.inp' for two components (ncp=2),  
 $qu_1 = 1 - qu_2$

number of layer	thick-ness	composition of target (2...ncp) qu_2	qu_3
200	5.0	0.3	0.7
300	5.0	0.7	0.3
0	0	0	0

Table 18: Inputfile 'layer.inp' for three components (ncp=3),  
 $qu_1 = 1 - sum(qu(2 : ncp)) = 0.0$

## D. Inputfiles 'energy.inp' and angle.inp

energy(eV)	distribution[-]
100	1
200	2
300	2
500	5
600	8
700	12
800	20
900	25

Table 19: Inputfile 'energy.inp'

angle(degree)	distribution[-]
30	10
60	20
70	20
90	70

Table 20: Inputfile 'angle.inp'

## E. Inputfiles 'ene\_ang.inp'

0.000000			: help	value			
0.000000			: help	value			
9			: columns	Angles			
10.0000	80.00000	10.00000	: Min Max	dAngle	[degrees]		
13			: rows	Energy			
10.0000	140.0000	10.00000	: Min Max	dE	[eV]		
2.39560	2.728417	9.982015	4.214628	1.330935	4.436451	3.327338	
1.55830	5.512290	1.098021	2.994604	2.218225	1.109112	0.000000	
3.56800	5.079736	3.438249	4.436451	2.218225	1.109112	0.000000	
3.32730	2.218225	1.109112	1.109112	1.109112	0.000000	0.000000	
0.000000	0.000000	0.000000	0.000000	0.000000	0.000000	0.000000	
0.000000	0.000000	0.000000	0.000000	0.000000	0.000000	0.000000	
0.000000	0.000000	0.000000	0.000000	0.000000	0.000000	0.000000	
0.000000	0.000000	0.000000	0.000000	0.000000	0.000000	0.000000	
0.000000	0.000000	0.000000	0.000000	0.000000	0.000000	0.000000	
0.000000	0.000000	0.000000	0.000000	0.000000	0.000000	0.000000	
0.000000	0.000000	0.000000	0.000000	0.000000	0.000000	0.000000	
0.000000	0.000000	0.000000	0.000000	0.000000	0.000000	0.000000	
0.000000	0.000000	0.000000	0.000000	0.000000	0.000000	0.000000	
0.000000	0.000000	0.000000	0.000000	0.000000	0.000000	0.000000	
0.000000	0.000000	0.000000	0.000000	0.000000	0.000000	0.000000	

Table 21: Inputfile 'ene\_ang.inp'



## F. Example of new Inputfile 'tri.inp'

Inputfile 'tri.inp' of first static example He - > Ni

2 keV He - > Ni  
& TRLINP

```
text='—elements—'  
  ncp = 2  
  symbol = "He", "Ni"  
  
  flc = 10.000E+0  
  nh = 10  
  idout = 10  
  nr_pproj = 1  
  
  idrel = 1  
  isbv = 1  
  ipot = 1  
  
text='—beam—'  
  qubeam = 1.000, 0.000  
  qumax = 0.000, 1.000  
  case_e0 = 0  
  e0 = 2000, 0.00  
  case_alpha = 0  
  alpha0 = 0.000, 0.000  
  
text='—target—'  
  ttargt = 5000E+0  
  nqx = 500  
  qu = 0.0 , 1.0  
  e_cutoff= 1.0 ,1.0  
  
  ltraj_p = .true.  
  ltraj_r = .true.  
  numb_hist = 1  
  ioutput_hist = 1, 1, 0, 1, 1, 0  
  lparticle_r = .true,  
  lparticle_p = .true.  
  ioutput_part = 100, 100, 0, 100, 100, 0
```

/

## Inputfile 'tri.inp' of second static example Ar - > Ni

1 keV Ar - > Ni

& TRIINP

text='—elements—'

ncp = 2

symbol = "Ar", "Ni"

flc = 10.000E+0

nh = 10000000

idout = 100000

nr\_pproj = 10

idrel = 1

ipot = 1

isbv = 1

text='—beam—'

qubeam = 1.000, 0.000

qumax = 0.000, 1.000

case\_e0 = 0

e0 = 1000, 0.00

case\_alpha = 0

alpha0 = 60.000, 0.000

text='—target—'

ttarget = 5000E+0

nqx = 500,

qu = 0.0 , 1.0

lmatrices = .true.

/

## Inputfile 'tri.inp' of first dynamic example Ni - > WC

10 keV Ni - > WC  
& TRI.INP

text='—elements—'

ncp = 3  
symbol = "Ni", "W", "C\_g"  
flc = 15.00  
nh = 50000  
idout = 500  
nr\_pproj = 32

text='—beam—'

qubeam = 1.000, 0.000, 0.000  
qumax = 1.000, 1.000, 1.000  
case\_e0 = 0  
e0 = 10000, 0.00  
case\_alpha = 0  
alpha0 = 0.0 , 0.000, 0.000

ipot = 1  
isbv = 3  
inel0 = 3

text='—target—'

nm=2  
two\_comp='WC'  
idrel = 0  
ttarget = 500  
nqx = 100  
qu = 0.0, 0.5, 0.5

/

## Inputfile 'tri.inp' of second dynamic example $W \rightarrow C$

5 keV  $W \rightarrow C$

& TRIINP

```
text='—elements—'  
  ncp = 2,  
  symbol = "W", "C_g"
```

```
  flc = 50.00  
  nh = 1000000  
  idout = 2000  
  nr_pproj = 32
```

```
text='—beam—'  
  qubeam = 1.000, 0.000  
  qumax = 1.000, 1.000  
  case_e0 = 0  
  e0 = 5000, 0.00  
  case_alpha = 0  
  alpha0 = 0.00, 0.00
```

```
  ipot = 1  
  isbv = 3  
  inel0 = 3
```

```
text='—target—'  
  idrel = 0  
  ttarget = 1000  
  nqx = 100  
  qu = 0.0, 1.0  
  iwc = 0  
  e_cutoff= 6.0, 6.0
```

/

### Inputfile 'tri.inp' of third dynamic example Ar - > Si Ta

```
3 keV Ar - > Si Ta
& TRLINP
  text='—elements—'
    ncp = 3,
    symbol = "Ar", "Si", "Ta"
    flc = 50
    nh = 100000
    idout = 1000
    nr_pproj = 10
    ipot = 1
    isbv = 3
  text='—beam—'
    qubeam = 1.000, 0.000, 0.000
    qumax = 0.000, 1.000, 1.000
    case_e0 = 0
    e0 = 3000, 0.00
    case_alpha = 0
    alpha0 = 0.000, 0.000 ,0.000
  text='—target—'
    idrel = 0
    nm=3
    ttargt = 1815
    nqx = 263
    qu = 0.0, 0.5, 0.5
    iq0 = -1
/
```

### Inputfile 'layer.inp' of third dynamic example Ar - > Si Ta

number of layer	thick- ness	target qu_2	composition 2...ncp qu_3	name of layer
40	5.00	1.0000	0.0000	Si 1
15	5.00	0.0000	1.0000	Ta 1
21	5.00	1.0000	0.0000	Si 2
15	5.00	0.0000	1.0000	Ta 2
21	5.00	1.0000	0.0000	Si 3
15	5.00	0.0000	1.0000	Ta 3
21	5.00	1.0000	0.0000	Si 4
15	5.00	0.0000	1.0000	Ta 4
200	5.00	1.0000	0.0000	Si 5
0	0	0	0	end

## Inputfile 'tri.inp' of sputtering with noble gas ions Xe - > Si

40 keV Xe - > Si

& TRI.INP

text='—elements—'

nep = 2,

symbol = "Xe", "Si"

text='—beam—'

case\_e0 = 0

e0 = 40000, 0.00

qubeam = 1.00, 0.000

case\_alpha=0

alpha0 = 0.0 , 0.000

text='—control—'

flc = 7

nh = 70000

nr\_pproj = 20

idout = 1000

idrel = 0

ipot = 1

iintegral=2

ipivot=8

text='—target—'

ttarget = 1000

nqx = 100

isbv = 3,

inel0 = 3 ,3

qu = 0.0, 1.00

qumax = 1.00, 1.000

dns0 = 0.01623, 0.04994

e\_cutoff= 1.0, 1.0

qu\_int= .true.

case\_layer\_thick=1

loutgas = .true.

diff\_koeff1 = 2.80e06 , 0.0

/

## Inputfile 'tri.inp' of sputtering with chemical erosion D - > C

200 eV D - > C

& TRI.INP

text='—elements—'

ncp = 4

symbol = "D", "Sp2", "Sp3", "Sp3H"

flc = 20

nh = 5000

idout = 50

nr\_pproj = 100

idrel = 0

isbv = 3

ipot = 1

iintegral=2

ipivot=8

text='—beam—'

qubeam = 1.00 , 0.00 , 0.00, 0.00

case\_e0=0

e0 = 200 ,0.00, 0.00, 0.00

case\_alpha=0

alpha0 = 0.00, 0.00, 0.00, 0.00

text='—target—'

ttarget = 5000,

nqx = 1000,

qumax = 1.0, 1.00, 1.00, 1.00

qu = 0.0, 1.00, 0.00, 0.00

ttemp = 300

e\_surfb = 1.00 ,7.37 ,5.00 ,5.00

e\_displ = 3.0 ,3.75 ,3.75 ,3.75

e\_cutoff= 1.0 ,1.0 ,1.0 ,1.0

qu\_int = .true.

case\_layer\_thick=1

loutgas = .true.

diff\_koeff1 = 0.20E06, 0.0, 0.0, 0.0

lchem\_ch = true

flux = 0.01

/